

---

# Imaging and Positioning of Objects at the Nanoscale

Christian Steinhauer

---



Munich, December 17, 2010



---

# Imaging and Positioning of Objects at the Nanoscale

---

Dissertation

Submitted by

Christian Steinhauer  
from Heidenheim a.d. Brenz

at

Faculty of Physics  
Ludwig-Maximilians-University  
Munich

Munich, December 17, 2010

Erstgutachter: Prof. Dr. Philip Tinnefeld  
Zweitgutachter: Prof. Dr. Tim Liedl  
Tag der mündlichen Prüfung: 25.01.2011

## Summary

The process of miniaturization brings benefits in many areas of every day life. It describes the process of down-scaling mechanical, optical and electronic devices while maintaining their function. This continuous process has brought up the field of nanotechnology. It allows computers to run faster and faster while reducing their size and energy consumption. Many bio-analytical applications profit from smaller sizes to be more sensitive with lower sample volumes. Finally, each and every living cell contains the most complex nanoscopic machinery.

In order to mimic nature's highly efficient concepts, they first of all need to be understood. Their nanoscopic dimensions, however, make this task a very challenging one. Direct observation of sub-cellular processes by conventional light microscopy is difficult as almost all cellular components are colorless. Fluorescence microscopy introduces sufficient contrast and can be specifically applied to many different target molecules but remains limited in its spatial resolution.

In this work, a new approach to increase the resolution of fluorescence microscopy is presented that is termed "blink microscopy". It is based on the subsequent localization of single molecules as it is realized in recent techniques known as STORM or PALM, but does not require special photoswitchable fluorophores or multiple lasers. Instead of photoswitching, reversible electron transfer reactions are used to generate the required dark states.

Motivated by the task to assess the resolution of blink microscopy, DNA nanotechnology is used for nano-construction of a calibration structure. The DNA origami technique, developed by Paul Rothemund in 2006, allows for arranging of individual fluorophores at distances of 1–100 nm on a DNA nanostructure. While it is impossible to resolve two spots at a distance below 200 nm with conventional fluorescence microscopy, it was possible to confidently resolve 50 nm with blink microscopy. These experiments prove both, blink microscopy to be able to reliably resolve small distances and DNA origami structures to be well suited as a rigid breadboard for fluorescence experiments.

This research pioneering the combination of the two powerful tools of nano-imaging and nano-construction set the ground for further experiments. After the rigidity of DNA origami structures was used to characterize a fluorescence technique, single-molecule fluorescence could also help to characterize properties of the DNA origami. Namely, dynamic processes on a DNA nanostructure were exemplarily studied by reversible binding of a fluorescently labeled DNA strand while observing this process in real-time on a fluorescence microscope. With the knowledge about binding and unbinding kinetics of DNA and imaging of single molecules, another super-resolution approach was developed that is simply and flexibly implemented in DNA structures, not limited by photobleaching, easy to extend to multiple colors and that shows potential for cellular imaging.



## Contents

<b>1</b>	<b>Introduction</b>	<b>1</b>
1.1	The trouble with small things . . . . .	1
1.2	Basic principle of localization microscopy . . . . .	2
1.3	On the importance of dark states . . . . .	3
1.3.1	Acquisition time . . . . .	4
1.3.2	Fraction of correct localizations . . . . .	5
1.3.3	Achievable resolution . . . . .	5
1.4	DNA nanotechnology and the DNA origami technique . . . . .	7
<b>2</b>	<b>Materials and Methods</b>	<b>9</b>
2.1	The microscope . . . . .	9
2.2	The DNA origami technique . . . . .	10
<b>3</b>	<b>Super-Resolution Microscopy on the Basis of Engineered Dark States</b>	<b>11</b>
3.1	Understanding and controlling fluorescent dark states . . . . .	11
3.2	Extending dark state lifetimes . . . . .	12
3.3	Applications of blink microscopy . . . . .	13
3.4	Associated Publication P1 . . . . .	15
<b>4</b>	<b>DNA Origami as a Nanoscopic Ruler for Super-Resolution Microscopy</b>	<b>16</b>
4.1	Bottom up assembly of nanoscopic structures . . . . .	16
4.2	Further developments of the nanoscopic ruler . . . . .	18
4.2.1	Smaller distances . . . . .	18
4.2.2	A nanoscopic ruler for STED microscopy . . . . .	18
4.2.3	Higher labeling densities . . . . .	18
4.3	Associated Publication P2 . . . . .	20
<b>5</b>	<b>Single-Molecule Kinetics and Super-Resolution Microscopy by Fluorescence Imaging of Transient Binding on DNA Origami</b>	<b>21</b>
5.1	Observing dynamic processes on DNA nanostructures . . . . .	21
5.2	Possible applications of DNA-PAINT . . . . .	21
5.2.1	DNA-PAINT for the characterization of DNA origami . . . . .	21
5.2.2	DNA-PAINT imaging applied to cellular structures . . . . .	22
5.3	Associated Publication P3 . . . . .	24

<b>6 Submitted manuscript: Four-Color Single-Molecule FRET Visualizes Energy Transfer Paths on DNA Origami.</b>	<i>25</i>
<b>References</b>	<i>25</i>
<b>Appendix</b>	<i>30</i>
<b>Appendix</b>	<i>31</i>
Supporting information for P1 . . . . .	<i>31</i>
Supporting information for P2 . . . . .	<i>38</i>
Supporting information for P3 . . . . .	<i>44</i>
Curriculum Vitae . . . . .	<i>62</i>
Full list of Publications . . . . .	<i>64</i>



# 1 Introduction

From the very beginning, the ability to intelligently design and construct functional entities has enabled technological progress. Over the last decades, due to limited resources, energy and space, the miniaturization of machines became a key issue for further progress. Integrated circuits constantly need to decrease in size in order to meet increasing data processing requirements. Many biological and medical applications rely on the functionality of proteins, the smallest machines known so far. These developments face some fundamental barriers which need to be overcome. Two such barriers are discussed in this chapter: the manipulation and the observation of objects at the nanometer scale.

## 1.1 The trouble with small things

Handling objects in our macroscopic world is very different from manipulating objects at the nanoscale. The construction of an object with a size of 10 cm is not a difficult task. Decreasing the size by a factor of a hundred ( $\rightarrow 1$  mm) already reaches the human limits of mechanical precision as well as optical resolution. With another 100-fold decrease in size, sophisticated tools are needed to create those structures and only a sensitive microscope is able to visualize them. Finally, with another factor of 100 to a size of 100 nm, there is no possibility whatsoever to directly manipulate or observe any structure and also indirect methods are very limited.

Current techniques of nanofabrication are mainly based on lithographic approaches where focused ions, electrons or light are used to remove material (usually photo resist) from a layered surface in a top down approach<sup>1</sup>. This way, features the size of several tens of nanometers can be achieved (figure 1.1). It is the basic technique for the construction of computer chips as it is well suited for metals and semiconductor materials.

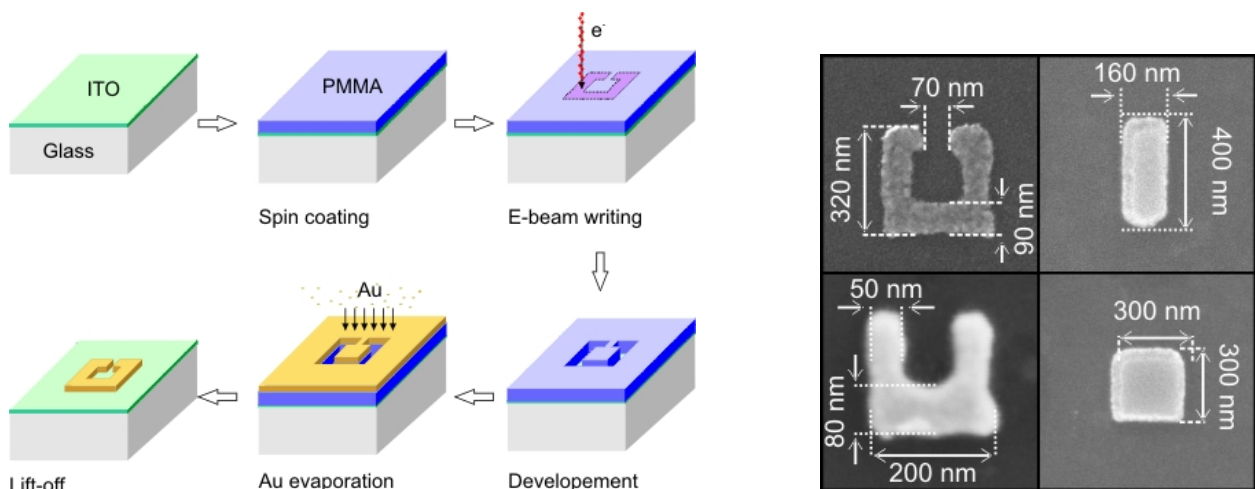


Figure 1.1: Top down approach of nano-lithography<sup>2</sup>

The limitations of lithographic approaches are their spatial resolution as well as the inability to combine different components other than stacking different layers on top of each other. An alternative way to create structures on the nanoscale is offered by the recently emerging field of DNA nanotechnology<sup>3</sup>. This comprises a bottom up approach with nanometer resolution and full addressability. New applications for DNA based nanosystems are presented in this work.

A major means of analyzing and inspecting structures is their visualization as an image. Electron Microscopy (EM) and Atomic Force Microscopy (AFM) are capable of imaging with atomic resolution. This extraordinary resolution however is accompanied by several technical limitations. EM only works on conductive materials or when stained with heavy metal ions and at high vacuum. AFM works at ambient conditions and in aqueous environments but can only probe the top surface of a sample and is likely to mechanically influence the sample while imaging it. Both techniques are not well suited for discerning different materials within a sample. All these disadvantages are absent in light microscopy, which is in turn strongly limited in its resolution due to diffraction. According to Ernst Abbe, visible light can only resolve objects with a distance of more than 200-300 nm. The minimum distance of two resolvable objects  $d$  depends on the wavelength  $\lambda$ , the refractive index of the imaging medium  $n$  and the half angle of the maximal cone of light that can pass through the objective of a microscope  $\alpha$ <sup>4</sup>:

$$d = \frac{\lambda}{2 \cdot n \cdot \sin \alpha} \quad (1.1)$$

During the last years, it was shown that this resolution limit can be circumvented with sophisticated fluorescence techniques, that are referred to as super-resolution (SR) microscopies. Two general concepts can be discerned, one based on targeted switching and readout, and the other based on stochastic switching and readout of the fluorescence information<sup>5-9</sup>. This work will solely focus on the latter which will henceforth be called localization microscopy.

## 1.2 Basic principle of localization microscopy

A single molecule fluorescing in an otherwise dark image can be localized with high precision depending on the number of photons it emits<sup>10</sup>. Although its emission is blurred in a point-spread-function (PSF), this function can be fitted with a two-dimensional Gaussian which yields the molecule's position.

Diffraction fundamentally limits far-field optical resolution when there is more than one object to be spatially distinguished within a diffraction limited area (figure 1.2). The task for super-resolution imaging is now to break down the problem of resolving multiple emitters to a solvable problem, in this case to localizing a single molecule. Provided a way to separate the emission of single fluorophores within a diffraction limited area in time (e.g. by sequential switching), each one can be localized with high precision. Each single emitter's position histogrammed in two dimensions yields a super-resolved image of the structure investigated (figure 1.3). In general, with the introduction of time as a new dimension, more information on the position of molecules can be obtained.

For SR imaging, it is important to consider the following aspects:

- **Mechanical stability:** With increasing resolution, the mechanical stability of the microscope must be higher as well. Thermal drift and vibrations in axial and lateral direction must be lower than the expected resolution of the image or corrected for by fiducial marks.
- **Imaging speed:** During the time of image acquisition, the sample must not move. Especially for imaging live - which also means moving - cells, this must be considered.
- **Label density:** The Nyquist criterion<sup>11</sup> applied to SR microscopy demands the distances between the probes to be at most half the desired resolution. Especially for conventional immunostaining this poses sterical limitations for very high resolutions.

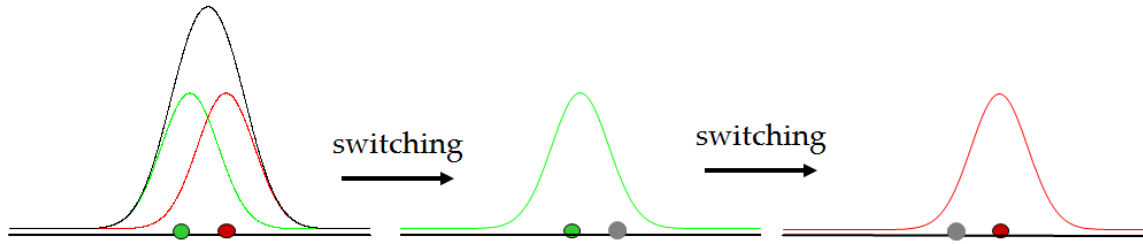


Figure 1.2: Principle of super-resolution imaging based on the subsequent localization of single molecules. The point spread functions of two fluorophores overlap, which makes discerning them impossible. Switched ON individually, each one can be localized.

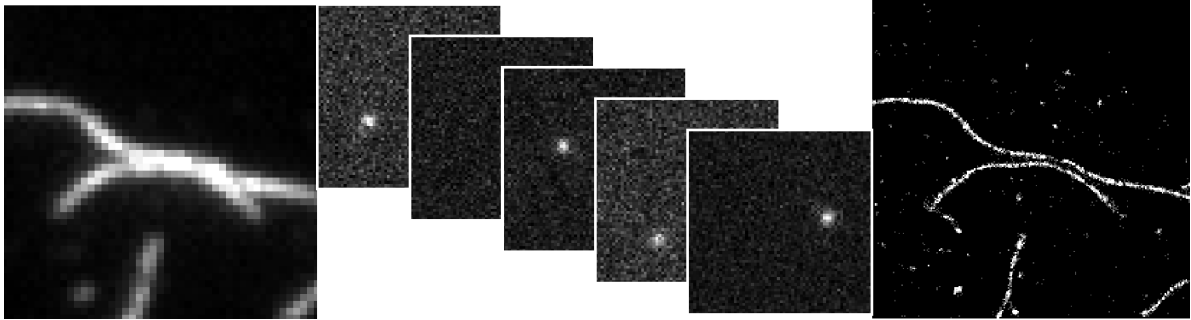


Figure 1.3: Example of a diffraction limited structure (actin filaments) and single molecule emission events. The right image shows the reconstruction of the left image after localizing individual positions from the single molecule images in the center.

Some parameters for SR imaging are relevant to localization microscopy in particular:

- **Number of photons ( $n$ ):** The precision of localizing a single molecule depends on the number of photons it emits while it is in its bright state. The standard deviation of the localization  $\sigma$  is the quotient of the standard deviation of each photon – which is given by the PSF – and the square root of the number of photons.
- **Ratio of ON and OFF times ( $\tau$ ):** A high ratio of  $\tau_{off}$  divided by  $\tau_{on}$  ensures that each emission event originates from a single molecule. The higher this ratio, the higher the likelihood of observing single molecule events which affects the achievable resolution especially in densely labeled samples<sup>12</sup>.

### 1.3 On the importance of dark states

The experimental resolution obtained by a localization based microscope depends on two almost independent parameters. One is the number of photons emitted by a fluorophore which directly determines the localization precision as mentioned before. The second parameter  $\tau$  influences several aspects that are explained in this section<sup>12</sup>.

From the characteristic times  $\tau_{on}$  and  $\tau_{off}$  and the number of molecules within a diffraction limited spot  $n$ , different probabilities can be calculated which are the basis for further calculations in this section (table 1.1).

$p_{on} = \frac{\tau_{on}}{\tau_{on} + \tau_{off}}$	Probability for a dye to be in its ON state in any given frame
$p_0 = (1 - p_{on})^n$	Probability that no molecule is active
$p_1 = n \cdot p_{on} \cdot (1 - p_{on})^{n-1}$	Probability that exactly one fluorophore is active
$p_{1corr} = p_1 \cdot p_0$	$p_1$ corrected for an ON time of one frame spread over two camera frames
$p_x = 1 - p_0 - p_1$	Probability of more than one dye being fluorescent

Table 1.1: Probability calculations.

### 1.3.1 Acquisition time

The minimum time needed to acquire a fully detailed image ( $n_{frames}$ ) depends on the number of molecules and the OFF time. Each dye must emit at least once as a single-molecule event. The more often a molecule is detected, the better the image quality. The recording time can be calculated with the following equation:

$$n_{frames} \geq a \cdot n \cdot p_{1corr}^{-1} \quad (1.2)$$

where  $a$  is the desired number of localizations per molecule. For the example of  $a = 5$ ,  $n_{frames}$  is plotted against  $\tau$  and  $n$  in figure 1.4. For most purposes, a short time for image acquisition is desired, so the OFF time should be adjusted - if possible - to be as low as possible while being sufficiently long to separate emission events in time. When a high number of frames is unavoidable, mechanical drift effects of the microscope must be taken into account.

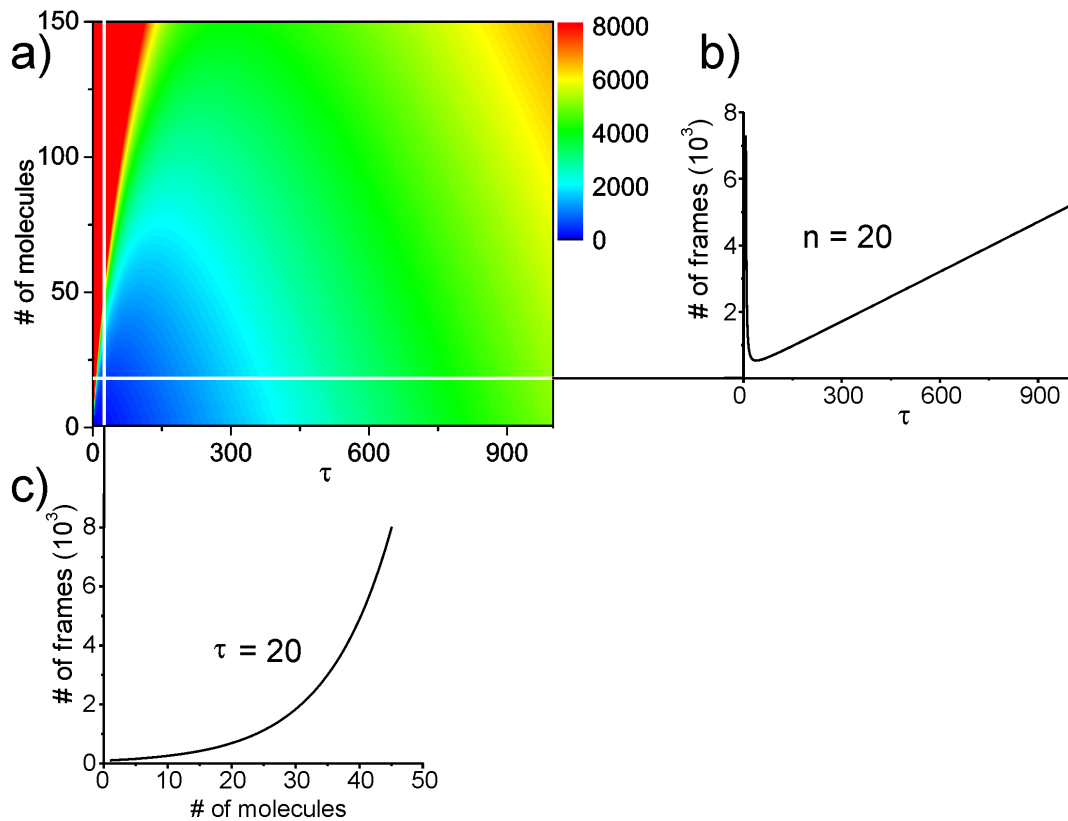


Figure 1.4: a) Number of frames to record to statistically detect each molecule at least five times for single-molecule localization. b,c) cross-section of graph a) for fixed values of  $n$  and  $\tau$ .

### 1.3.2 Fraction of correct localizations

Another characteristic resulting from  $\tau$  is the fraction of correct localizations. The equations in chapter 1.3.1 only describe how many frames are needed to get a sufficient number of *correct* localizations, meaning fluorescence events where *exactly one* dye is fluorescent. At the same time, there can be events where multiple fluorophores emit light within one PSF generating localizations of their superposition. This happens with a probability  $p_x$ . To obtain a meaningful image, the number of such “wrong” localizations, must be lower than the number of correct localizations.

The ratio of correct and biased localizations can be expressed as the ratio of the probabilities  $p_{1corr}/p_x = \rho$ . For  $\tau = 20$ , the progression of  $\rho$  is plotted against the number of molecules per PSF in figure 1.5.

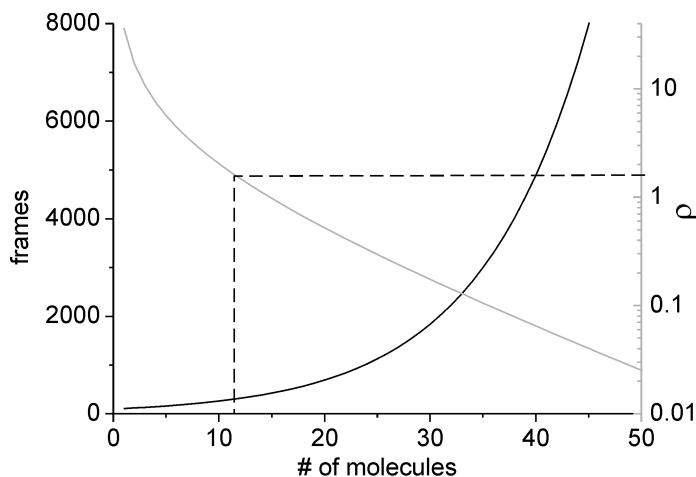


Figure 1.5: Minimal recording time and fraction of correct localizations in dependence of the number of molecules for  $\tau = 20$ .

The position  $\rho \approx 1.5$  is indicated by the dashed line, this is a reasonable value to obtain an image with a sufficient signal-to-noise ratio. Imaging at conditions below that line will most likely result in a too high number of artifacts in the super-resolved image. The recording time can of course be arbitrarily longer than the intersection with the horizontal dashed line, but this intersecting point is recommended as a reasonable value. The resulting maximum number of molecules per PSF that can be confidently resolved is 11. For different OFF times this maximum number is plotted in figure 1.6. The curve progression shows a surprising behavior as it follows a straight line with a slope of 0.6. The maximum number of temporally separable molecules  $n_{max}$  can be estimated with a simple equation after the combination of the equations in table 1.1:

$$n_{max} \approx \frac{\tau}{\rho} \quad (1.3)$$

### 1.3.3 Achievable resolution

The number of molecules resolvable in time indirectly affects the possible resolution. This strongly depends on the arrangement of fluorophores present in the investigated structure.  $\tau$  limits the resolution if many fluorophores are relatively evenly distributed within the PSF (figure 1.7 a). Alternatively, few dye molecules can occur at very dense clustering in which case the localization accuracy  $\sigma$  becomes crucial (1.7 b). In most cases, a combination of  $\tau$  and  $\sigma$  determine the resolution

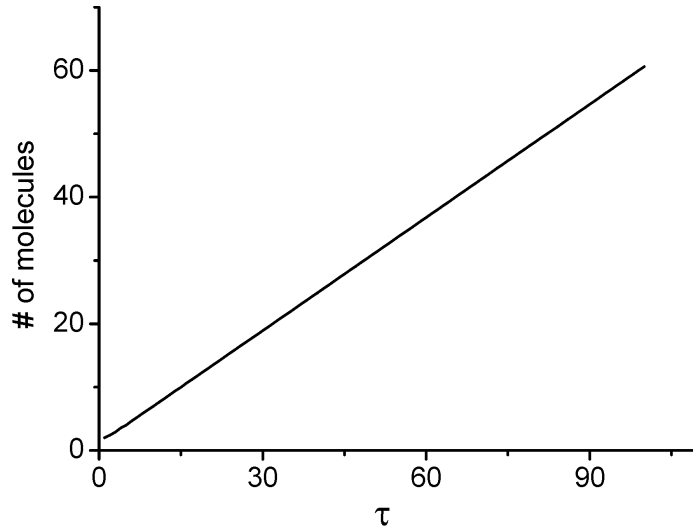


Figure 1.6: Maximum number of temporally resolvable molecule vs.  $\tau$ .

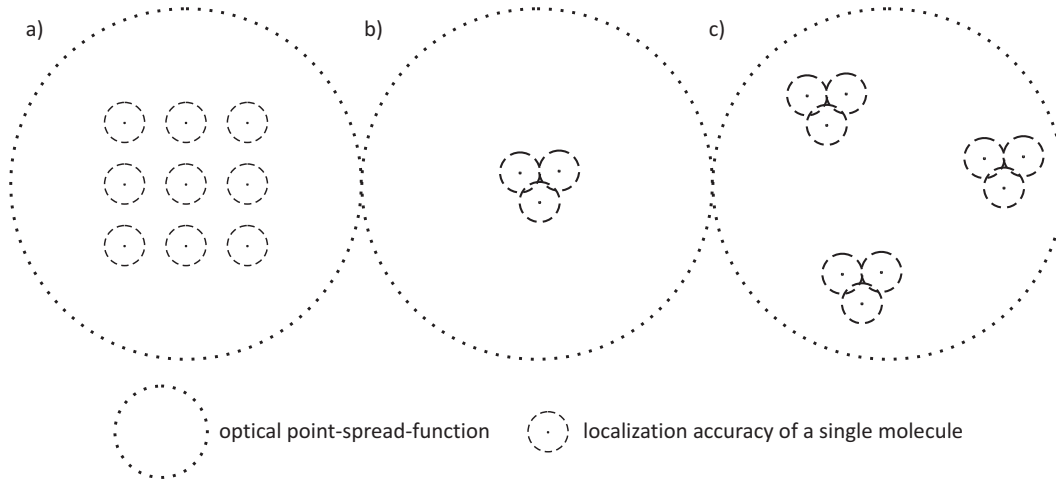


Figure 1.7: Possible distributions of single molecules within a PSF.

(1.7 c) of any localization based SR approach. For a theoretical description of  $\tau$ -limited resolution, a grid of single molecules with a certain grid constant  $d$  is considered. This arrangement describes the “worst case” in terms of temporal separation with least dependence on the localization accuracy and therefore defines an upper limit of what can be resolved in any given structure. The minimal grid distance is given by

$$d = \frac{FWHM \cdot \pi}{\sqrt{n} \cdot 4}. \quad (1.4)$$

These values are plotted together with Monte Carlo simulations performed in associated publication P1 (red squares in figure 1.8). The limit given in this graph is valid for a given ratio  $\tau$ . It represents the highest possible resolution in the most general case of fluorophore arrangements, meaning that there can be samples with higher resolution if the fluorophores are not evenly distributed.

In this context, it is also important to consider the Nyquist sampling theorem which poses additional requirements to the sample labeling. In essence, the theorem requires the sampling rate of a signal to be at least twice as high as the highest frequency of the signal. Transferred to SR imaging, this means that the pixel size of the super-resolved image must be half the desired resolution or

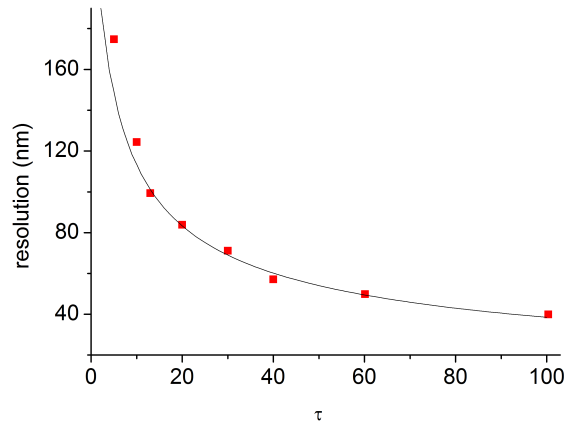


Figure 1.8: Theoretical limit of  $\tau$ -limited resolution and Monte Carlo simulations of diffraction limited grids of fluorophores.

smaller. For localization based microscopy the resulting “image” is a histogram with arbitrarily chosen bins, so the pixel size can be changed easily in the post-processing. However, the Nyquist theorem applies to the labeling of the structure itself. Assuming two parallel lines (e.g. tubulin in a cell) at a distance  $d$ , the distance between labels along those lines must be lower than  $d/2$  to confidently resolve the structure.

#### 1.4 DNA nanotechnology and the DNA origami technique

In a technical context, DNA, the carrier molecule of our genetic information, is a polymer with unique properties. Not only is it very stable, robust, flexible and easy to handle, it also contains information in its sequence. When DNA is used as a building material, it contains a blueprint for the structure to build. The sequence of the four nucleobases adenine (A), cytosine (C), guanine (G) and thymine (T) which only bind in the combinations of C and G as well as A and T (neglecting unlikely non Watson-Crick base pairing), determine which components of a structure are connected. Figure 1.9 gives a short historic overview from the most basic structures made from DNA to complex two and three dimensional constructs several hundred nanometers in size. Bottom up assembly of nanostructures from DNA offers several advantages. Most importantly, the inherently encoded information allows parallel self assembly of specific structures of high complexity. To functionalize the new material, many chemical and biological modifications are commercially available. The building blocks themselves can be produced at low cost by synthesis or by extraction from biological samples like the genome of phage M13mp18 which is used for the DNA origami technique developed by Paul Rothemund<sup>17</sup> in 2006.

He introduced the idea to use viral single-stranded DNA with a known sequence as a scaffold for assembling an ordered structure. This scaffold of about 7000 bases is used to connect a set of 226 so called staple strands. This way the staple strands no longer need to be complimentary to each other and hence be present at equal concentrations, but they can be used in high molar excess over the scaffold.

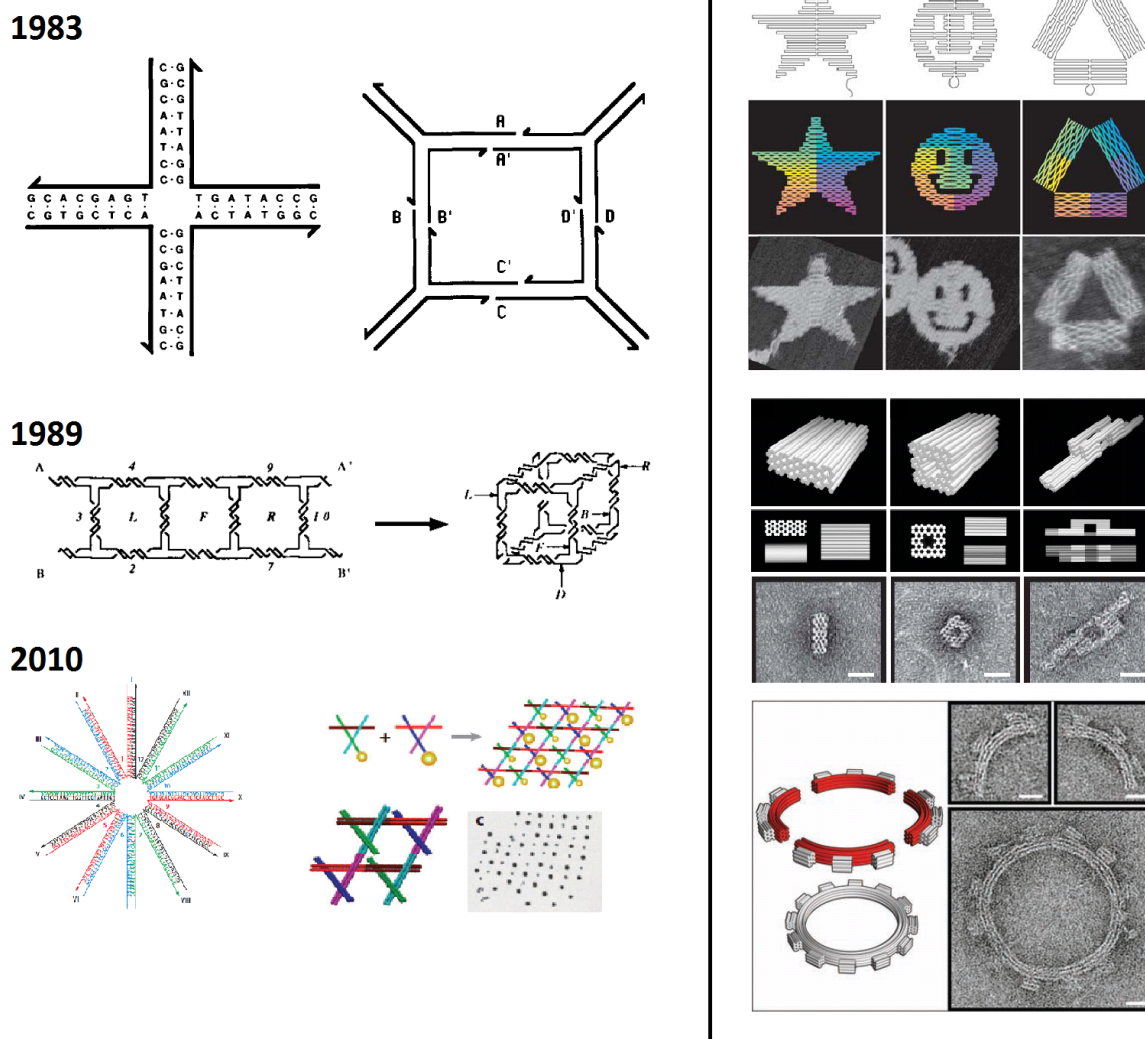


Figure 1.9: DNA as a building material for nanotechnology. The left panel shows the increasing complexity of DNA structures by Nadrian Seeman. The right panel shows the DNA origami technique developed by Paul Rothemund and its extensions to three dimensional structures<sup>13–19</sup>.

A simple gedankenexperiment elucidates this key issue in self assembly processes: A self-assembling system consisting of 3 building blocks AB, BC and CD can form a trimer where identical letters are connected. When the coupling efficiency is only 50%, BC must be present twice as much as AB to achieve full hybridization of AB. This however leaves a surplus of unconnected BC. For component CD, the same is true in respect to BC, so in total it must be 4 times more CD in the reaction than AB. For a system of 200 components and 95% coupling efficiency, the last component must at least be at 16469 times higher concentration than the first. With the help of a scaffold ABBCCD... that connects all the components of a structure, a constant excess of each component over the scaffold is sufficient.

For the folding process of DNA origami structures, a 5–10 fold excess of each staple yields a very high fraction of well formed structures. In this work DNA origami rectangles with different modifications are used to characterize super-resolution fluorescence microscopy techniques and in turn, single-molecule fluorescence is used to characterize these structures.



## 2 Materials and Methods

### 2.1 The microscope

All fluorescence experiments described in this work were performed on a custom made total internal reflection fluorescence (TIRF) microscope based on an inverted Olympus IX71. Details of the setup for the individual experiments can be found in the respective supporting information file attached to this manuscript. A general schematic is given in figure 2.1. Two lasers beams are overlaid with a

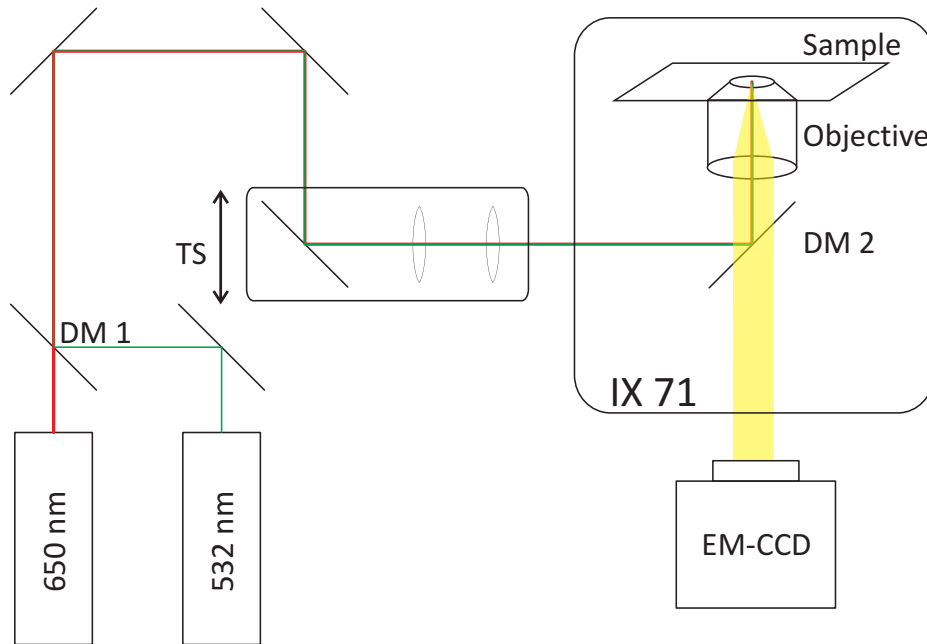


Figure 2.1: Schematic of the fluorescence microscope used for the experiments.

dichroic mirror (DM 1) and coupled into a commercial microscope (IX 71). Before the beam enters the microscope, it is expanded and focused by two lenses in a translation stage (TS). These lenses focus the light to the back focal plane of a high numerical aperture objective (NA 1.40) which generates a homogeneous wide-field illumination in the sample. The translation stage laterally moves the beam from the center of the back aperture of the objective towards the edge which makes the light exit the objective in a lower angle until total internal reflection is reached at the cover glass surface. Fluorescence light is separated from the excitation light by another dichroic mirror (DM 2) and imaged with an electron multiplying CCD camera (EM-CCD).

Data was recorded with the software provided by the manufacturer and analyzed with a self-made software written in LabView.

## 2.2 The DNA origami technique

The scaffold used for folding the origami structures is taken from the bacterio-phage M13mp18. Usually, 3 nM of scaffold is combined with a mixture of individually synthesized staple strands at a concentration of 50–100 nM. Defined staples were replaced with fluorescently labeled DNA depending on the purpose of the experiment. This mixture was heated in a thermocycler to 95°C and slowly cooled down within two hours. The high temperature eliminates all secondary structure of the DNA while the long cooling process ensures that each position of the scaffold gets annealed to the thermodynamically most favored staple strand. This way it folds into the structure prescribed by the sequence of the staples.

All DNA origami objects used in this work were designed as flat two-dimensional structures. For immobilization to a BSA/streptavidin coated surface, multiple biotinylated staple strands were introduced. These were designed such that the biotin anchors extrude from the origami structure on one side, thus defining a bottom side, while all relevant fluorescence modifications were attached on the top surface.

The DNA origami rectangle used in associated publication P2 is taken from Rothemund’s original publication<sup>17</sup>. In this design, each staple connects three helices of the scaffold as schematically shown in figure 2.2. It also features a bridged seam along the center.

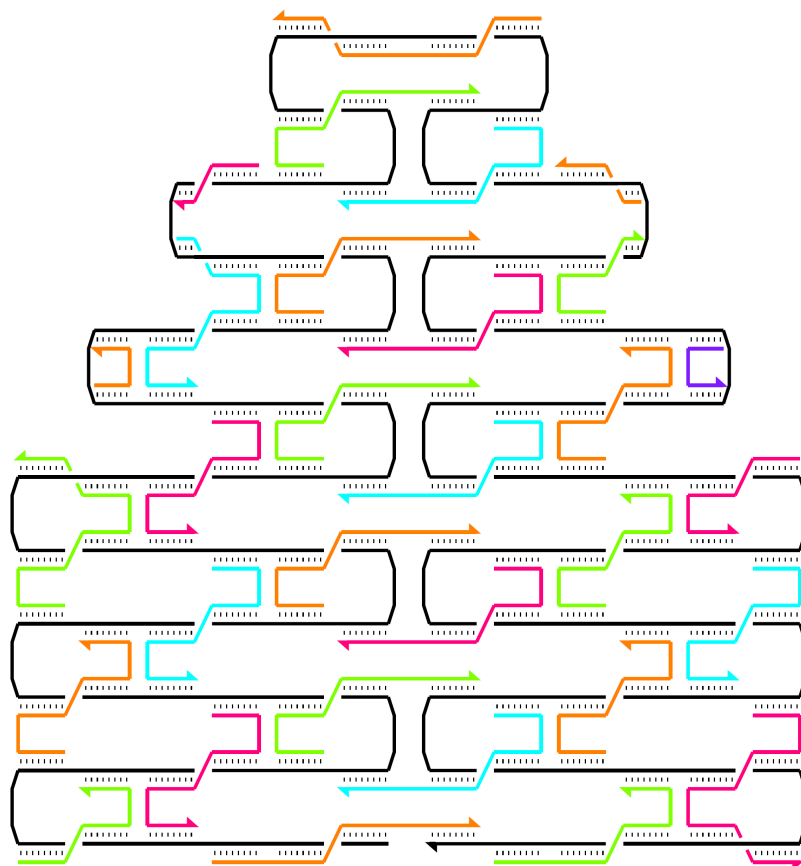


Figure 2.2: Design principle of DNA origami structures used in this work<sup>17</sup>.

The elongated rectangle for publication P3 is based on the same design but with a higher aspect ratio to obtain longer structures. The staple sequences were calculated with caDNAno, a software for the design of three-dimensional DNA origami nanostructures<sup>20</sup>.

### 3 Super-Resolution Microscopy on the Basis of Engineered Dark States

#### 3.1 Understanding and controlling fluorescent dark states

The major task in performing localization based SR microscopy as described in chapter 1.2 is the generation of single-molecule emission events separated by time. The first switching mechanism for organic fluorophores used in SR microscopy<sup>7,21</sup> is the reversible switching of the cyanine dye Cy5 with two different wavelengths of light. At that time, the exact mechanism of this switching was not well understood and was three years later revealed to be the reversible addition of a thiol to the fluorophore's delocalized electron system<sup>22</sup>. A more general approach is the use of triplet blinking. This ON and OFF switching is intrinsic to all organic fluorophores. It results from a spin conversion of the electron in the excited state  $S_1$  as shown in figure 3.1. This process called intersystem crossing appears at a dye specific rate  $k_{ISC}$  and is converted back to the ground state  $S_0$  at a rate  $k_T$ . This triplet state is usually quenched by oxygen, however when oxygen is removed,

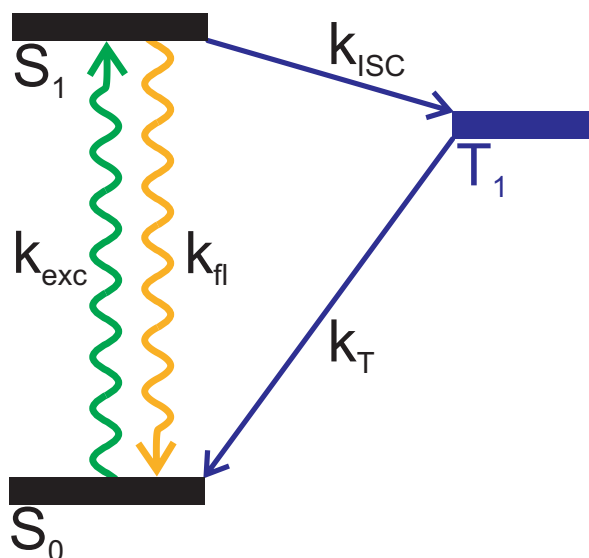


Figure 3.1: Jablonski diagram showing the transition to the triplet state.  $k_{exc}$  and  $k_{fl}$  are the fluorescence excitation and emission rates of the fluorophore.

the triplet state has a lifetime in the low millisecond range. For low label densities, this is already sufficient to be used as dark states for SR microscopy<sup>23</sup>. For working at higher, biologically relevant label densities, longer lived dark states are required.

To generate such dark states, extensive knowledge about the photophysics of fluorophores is needed. For example, blinking can also be due to, or induced by, electron transfer reactions of the dye<sup>24</sup>. The diagram in figure 3.1 must be extended accordingly (figure 3.2, left panel). The two states  $R^{\bullet-}$  and  $R^{\bullet+}$  are created from the triplet state by a reductant or oxidant which is present in solution. The fluorophore remains in that state until the respective counter-redox-agent transforms it back to its ground state. This mixture of reducing and oxidizing agents present at the same time eliminates blinking of many fluorophores and drastically increases their photostability as it efficiently depopulates the triplet state which could otherwise lead to photobleaching. The reducing and oxidizing agents do not react with each other because their redox potentials do not allow an efficient reaction, but they can react with fluorophores in their energy-rich excited state.

These newly identified redox states of fluorophores are employed for super-resolution microscopy

in associated publication P1 (chapter 3.4). Therein, the kinetics of switching are investigated and artificial as well as biological samples are imaged at sub-diffraction resolution with unprecedented speed. To achieve long-lived photoinduced dark states for SR microscopy, only one part of the reducing and oxidizing system (ROXS) is employed to trap a fluorophore in its reduced radical ion state  $R^{\bullet-}$  (see figure 3.2, right panel).

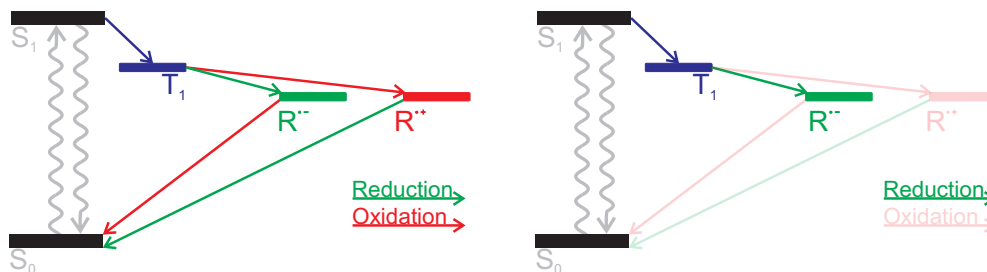


Figure 3.2: Jablonski Diagram showing the transition to the triplet state and to reduced and oxidized radical states according to the ROXS concept<sup>24</sup>. The right panel depicts the conditions for SR imaging where no or only a very low concentration of oxidant is present.

With the addition of the reducing agent ascorbic acid (AA) and removal of oxygen, which is an oxidizing agent, the OFF time  $\tau_{off}$  of Cy5 for example, increases from 14 ms (lifetime of the triplet state) to about 60 ms. The number of photons emitted during each on-cycle remains constant which indicates that the reductant does not act on the dye in  $S_1$  but that a transition to the triplet state is necessary for the reduction.

With the ambition of increasing the ratio  $\tau$  further,  $\tau_{on}$  should be as low as possible. This was achieved by high light intensities. An  $Ar^+Kr^+$  laser in single line mode ( $\sim 100$  mW) was used to illuminate a relatively small area of approximately  $100 \mu m^2$  which yields some  $kW/cm^2$ . In combination with a fast acquisition rate of 500-1000 Hz, the radical anionic dark state of Cy5 and other fluorophores can be used for SR microscopy.

This technique is called blink microscopy as it is based on single-molecule blinking. Due to the stochastic re-activation of fluorophores by oxidants diffusing in solution, it only requires a single laser for switching. It is not limited to special “photoswitchable” dyes but in principle works with any synthetic single-molecule fluorophore. As a side effect of the fast camera frame rate, the imaging speed is higher than in any other localization based super-resolution approach. Meaningful images can be recorded within just one second. This can be further improved with the development of faster cameras like the new Andor sCMOS camera. In addition the label density can be higher as  $\tau$  can be further increased by the shorter ON time.

### 3.2 Extending dark state lifetimes

Blinking is present in many classes of dyes. The blinking kinetics, however, differ strongly depending on the redox potentials of the radical states. Successful implementation of blink microscopy was shown for the cyanine dyes Cy3b and Cy5 in P1.

In later experiments, the oxazine derivate Atto655 showed particularly interesting characteristics. The energy of its reduced state is just slightly higher than the ground state. As a consequence, this state is much more stable and can hardly be oxidized by oxygen. Thus, SR imaging is possible also in the presence of oxygen with OFF times of several hundred milliseconds. When oxygen is

removed, practically infinite OFF times can be achieved<sup>25</sup>. In addition, the reducing agent can also depopulate the excited state and this way influence the number of photons emitted which directly determines the ON time. Hence, this dye offers a wide control of the ratio of ON and OFF times  $\tau$ .

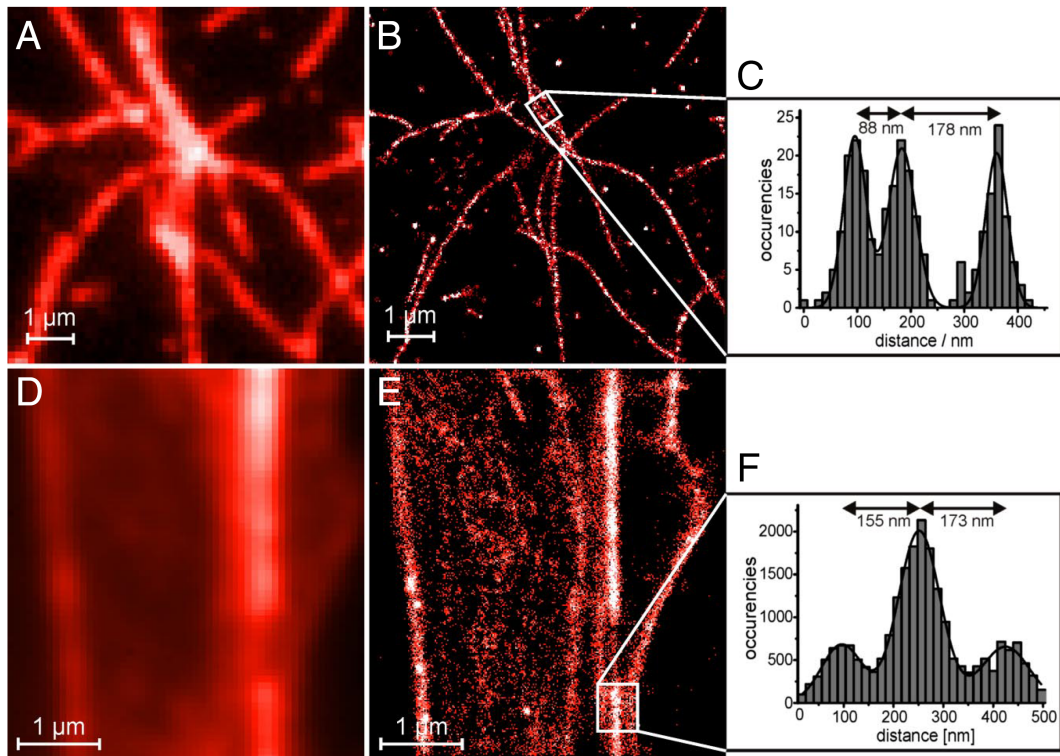


Figure 3.3: Diffraction limited and SR images of actin structures assembled in vitro (A-C) or in fixed cells (D-E)<sup>25</sup>.

### 3.3 Applications of blink microscopy

This fluorophore with improved blinking kinetics was used for convenient SR imaging in several publications<sup>25-27</sup>. An example showing actin filaments is given in figure 3.3. Another yet unpublished application of Atto655 for super-resolution imaging is the investigation of membrane clusters. In collaboration with Prof. Ken Jacobson from the university of North Carolina, the distribution of DC-SIGN, a receptor protein involved in carbohydrate recognition of immune cells<sup>28</sup>, was explored at the nanoscale. These receptors form up to micron-sized clusters in the cell membrane. They are of extraordinary stability, however their exact spatial composition cannot be examined in detail due to diffraction.

Fixed dendritic cells expressing DC-SIGN were immunostained with Atto655 conjugated to a secondary antibody. Blink microscopy images were recorded in the presence of oxygen. The results show clearly, that DC-SIGN receptors do not feature a homogeneous distribution within a cluster, but form substructures, mostly 2-3 subclusters consisting of one or more receptors each. An example is shown in figure 3.4. Currently analysis is performed on the size and lateral distribution of these substructures.

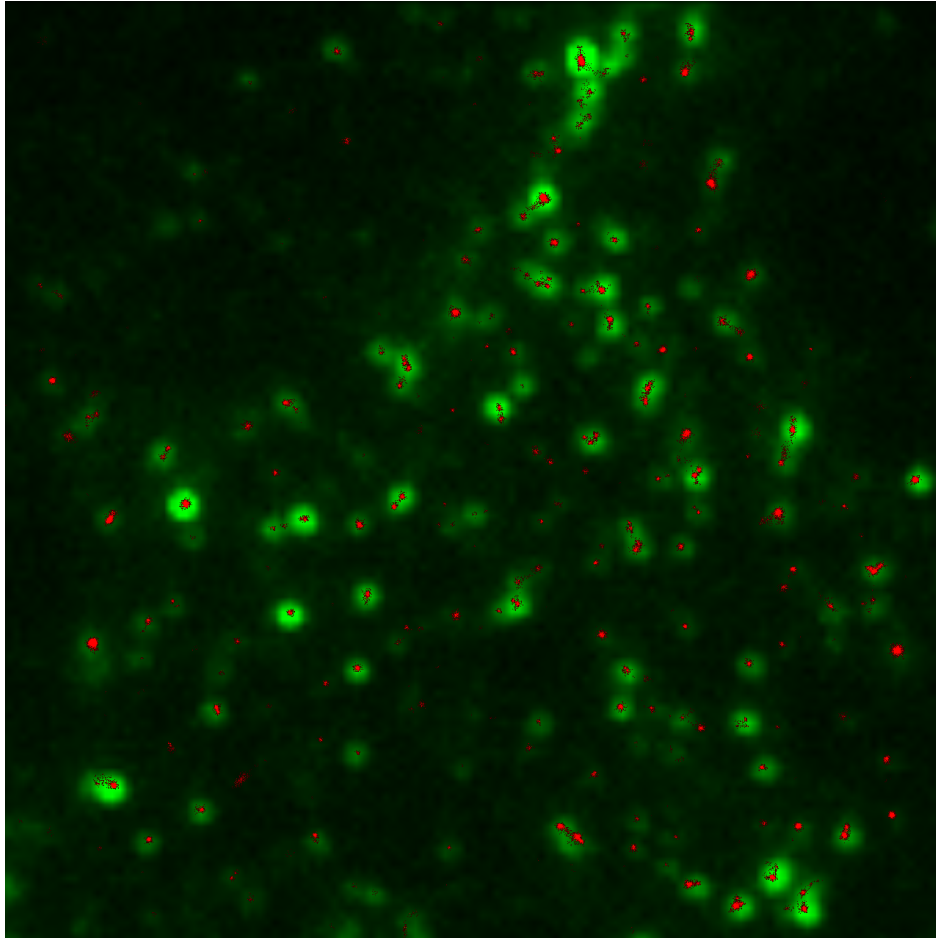


Figure 3.4: Overlay of diffraction limited (green) and super-resolution (red) images of DC-SIGN clusters in dendritic cells.

### 3.4 Associated Publication P1

## Super-Resolution Microscopy on the Basis of Engineered Dark States

By

C. Steinhauer, C. Forthmann, J. Vogelsang and P. Tinnefeld

published in

Journal of the American Chemical Society, 130(50):16840–16841

## 4 DNA Origami as a Nanoscopic Ruler for Super-Resolution Microscopy

### 4.1 Bottom up assembly of nanoscopic structures

During the last years, a multitude of publications on different approaches and applications of SR microscopy have emerged. Their superior resolution is well demonstrated. However, in most cases it is not possible to determine the experimental limit of the achievable resolution. Usually, randomly occurring structures in biological samples (e.g. tubulin filaments) are imaged and either their width or distance to each other is referred to as the resolution possible with the respective method. This, however, depends on the “luck” of the experimenter whether he can find a structure that exhibits the smallest resolvable detail. Furthermore, this way it is impossible to predict the resolution in a different structure that is more (or less) densely labeled.

To objectively compare different methods, a measure for the practically achievable resolution is required. While it is relatively simple to quantify the localization precision by investigating a single emitter, it is substantially harder to experimentally determine the influence of  $\tau$ . To do so, a well defined nanometer sized pattern of fluorescent molecules is required.

A sophisticated and flexible way to create such patterns is by “Single Molecule Cut-and-Paste” (SMCP) surface assembly with the help of an AFM<sup>29</sup>. A DNA functionalized AFM tip can pick up a complimentary DNA from a depot area, transport it to a target area and deposit it there with high precision (figure 4.1). The necessary hierarchical force system is designed into the DNA sequences that bind either in a zipper or shear geometry in the depot and target area, respectively.

It was possible to technically combine this technique with a super-resolution fluorescence microscope and quantify the effects of labeling density and  $\tau$  on the resolution<sup>27</sup>.

SMCP is a serial approach that writes one pattern at a time where each pattern can be chosen arbitrarily. For this study, this flexibility is used to create a multitude of different patterns and label densities to demonstrate the trade-off of acquisition speed and spatial resolution.

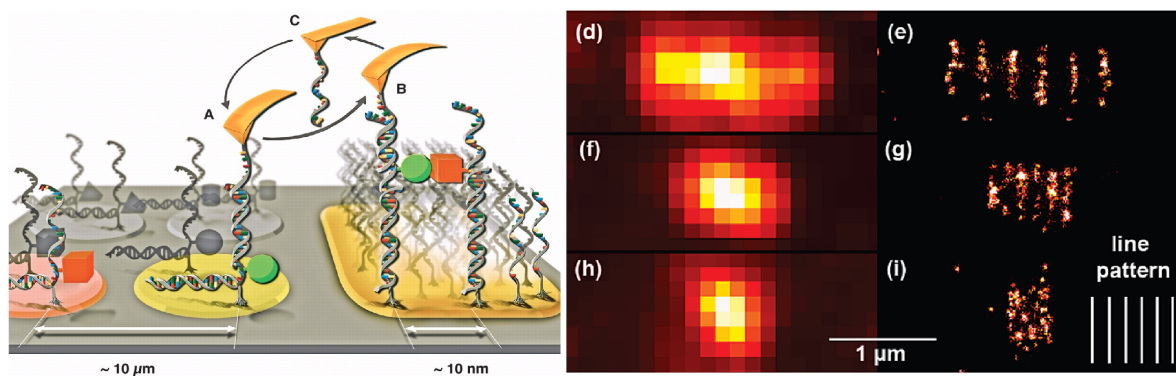


Figure 4.1: Left panel: Schematic principle of SMCP. A DNA functionalized AFM cantilever picks up DNA in a depot area (A) and transports it to a desired target (B) where it releases its cargo. It is then in its native state (C) where it can be re-used to transport the next molecule. Right panel: Diffraction limited (d,f,h) and super-resolved (e,g,i) images of line patterns created with SMCP.



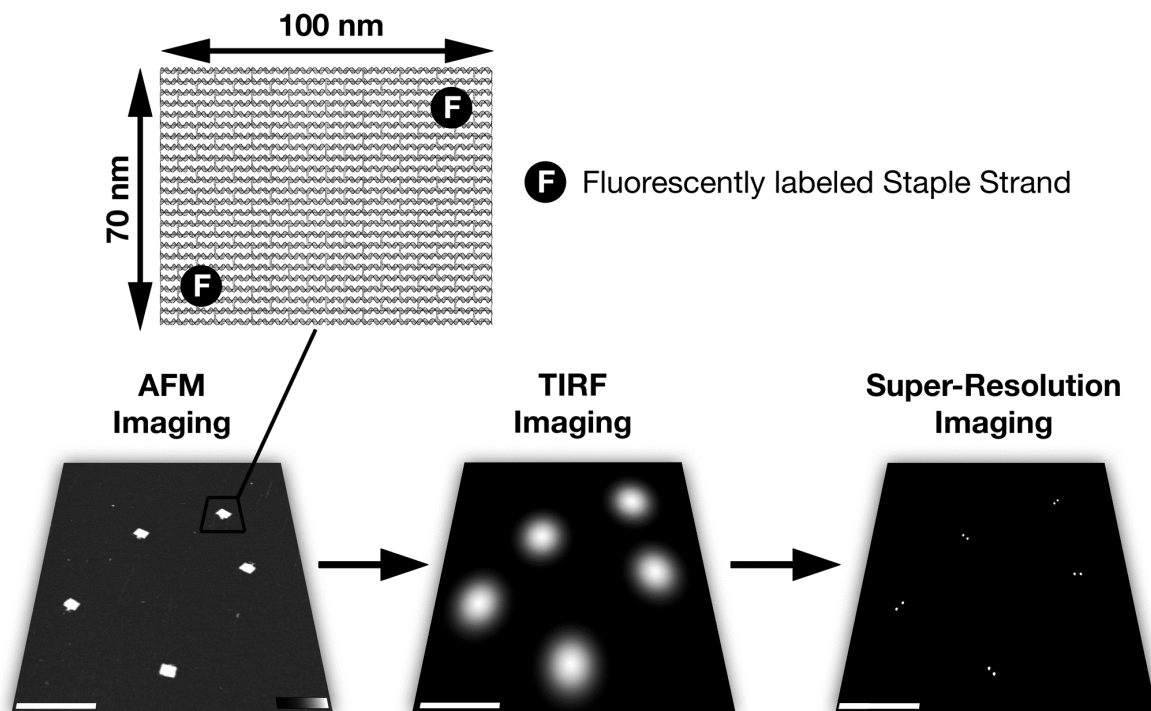


Figure 4.2: Schematic representation of the nanoscopic ruler. The top panel shows the placement of fluorophores on the origami rectangle. An AFM image reveals the structure of the origami rectangle while the fluorescence image yields diffraction limited blurred spots. A super-resolved image however reveals the position of the two dyes on the origami.

A fundamentally different approach is presented in associated publication P2 (chapter 4.3). It uses self-assembled DNA origami (see chapter 1.4 and figure 4.2) as calibration probes for super-resolution microscopy. It is possible to use these structures as breadboard to position fluorophores at distances of about 6 nm. Simply replacing any of the staple strands by a strand that is covalently coupled to a fluorophore, results in the fluorophore being positioned where the respective staple is placed in the folded structure. This way, an arbitrary pattern of fluorophores can be placed on a lattice of about 100 x 70 nm (figure 4.3).

To test the resolution of blink microscopy, the most fundamental pattern to do so is two points at a distance below the diffraction limit. This is realized with two fluorophores attached at opposing corners of a DNA origami rectangle at a distance of 90 nm.

Compared to the SMCP approach, DNA origami structures are less flexible. For each pattern, a different set of fluorescent staple strands needs to be purchased. However, once all the components are designed, these self-assembled calibration structures offer several advantages. They form in a 2-hour procedure that does not require time consuming surface preparation nor expensive AFM equipment. It results in billions of identical structures that are stable for many months. Immobilized on a glass surface, they can be subjected to different SR approaches in high numbers. The extraordinary yield of correctly folded structures and the high precision of placing fluorophores on the origami make them the ideal tool to test the resolution of any fluorescence microscope.

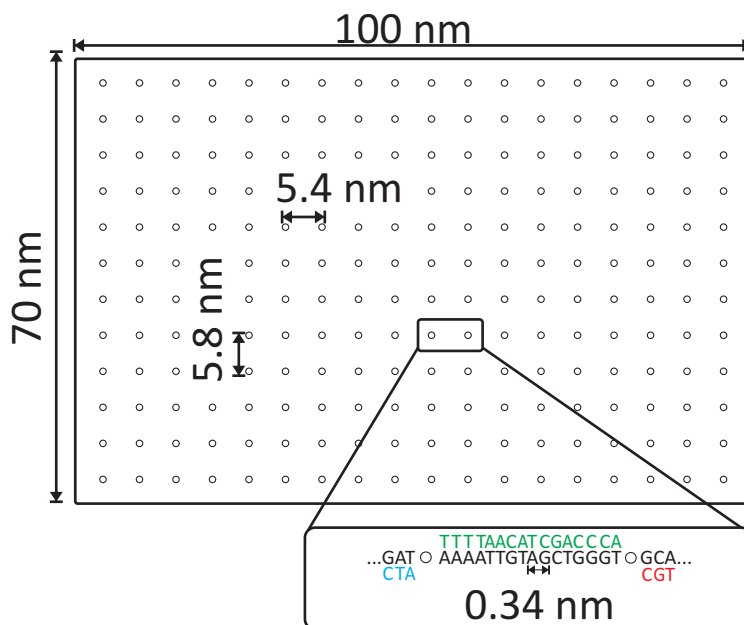


Figure 4.3: Schematic representation of a rectangular DNA origami. Each of the positions can contain a modified staple strand<sup>26</sup>.

## 4.2 Further developments of the nanoscopic ruler

### 4.2.1 Smaller distances

After the proof-of-principle experiments of P2 showed that DNA origami are sufficiently precise and robust structures for SR microscopy, they were used to assess the experimental limit of blink microscopy. To save costs, the staple strands chosen for distance measurements were purchased without modification, only extended with additional bases that are not complimentary to the scaffold strand. This way, a single stranded sequence at the origami surface is available for hybridization of fluorescently labeled DNA after the origami has folded. This method did produce the anticipated structures, however the yield of DNA origami that carried two fluorophores was very low. The results for nanoscopic rulers with fluorophore distances of 81 and 54 nm are displayed in figure 4.4.

### 4.2.2 A nanoscopic ruler for STED microscopy

In collaboration with Leica Microsystems, a nanoscopic ruler compatible with STED microscopy was developed. For high resolution measurements, STED requires high laser intensities and hence high photostability of the fluorophores. Imaging a single molecule at high resolution is possible but requires additional stabilization of the fluorophores<sup>30</sup>. Therefore, line structures with 12 dyes per line at a distance of 70 nm were produced (figure 4.5). These structures are currently investigated at Leica Microsystems, Mannheim.

### 4.2.3 Higher labeling densities

DNA origami structures offer more than 200 attachment sites for fluorophores. This facilitates precise investigation of the effects of  $\tau$  on resolution and image acquisition time (see chapter 1.3). Currently experiments are conducted on DNA origami with a full set of staple strands that can be addressed by diffusing fluorophores as described in the next chapter.

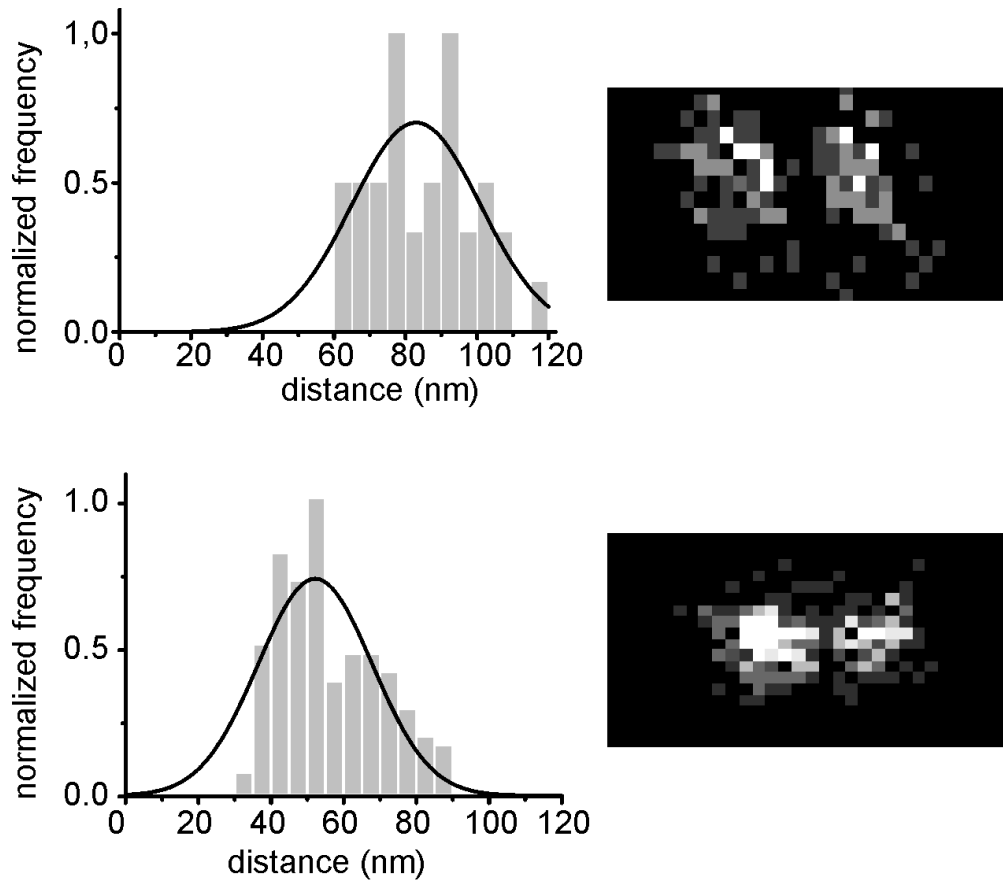


Figure 4.4: Distance distributions of fluorophores on DNA origami structure at a theoretical distance of 81 nm ( $n=40$ ) and 54 nm ( $n=100$ ) with typical super-resolution images of the respective samples.

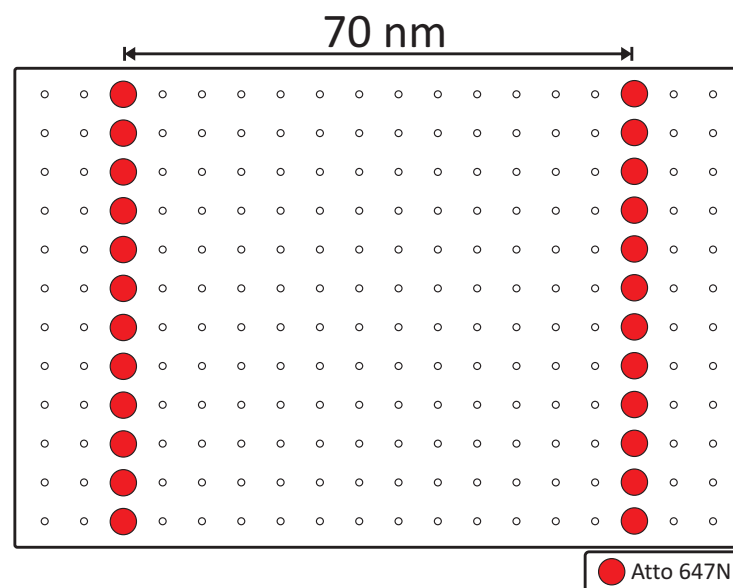


Figure 4.5: Design schematic of a nanoscopic ruler for STED microscopy.

### 4.3 Associated Publication P2

## DNA Origami as Probes for Super-Resolution Microscopy

By

C. Steinhauer, R. Jungmann, T.L. Sobey, F.C. Simmel and P. Tinnefeld

published in

Angewandte Chemie International Edition, 48:8870–8873

## 5 Single-Molecule Kinetics and Super-Resolution Microscopy by Fluorescence Imaging of Transient Binding on DNA Origami

### 5.1 Observing dynamic processes on DNA nanostructures

The construction of nanoscopic objects entails their functionalization as the next logical step. With the future perspective of building nanoscopic machines that are able to process information, detect and analyze biological samples at very low concentration or convert energy at high efficiency, new ways of characterizing those structures must be developed. In 2010, multiple publications investigated dynamic processes on DNA origami structures<sup>31-35</sup>. All these studies have in common that they rely on AFM imaging to read out the information. The obvious advantage of this method is its superior resolution and the AFM expertise and equipment present in any laboratory that works on DNA nanostructures. However, standard AFM cannot detect binding of small or flexible molecules and does not have the time resolution necessary for many experiments. Furthermore, the AFM cantilever is likely to interact with the sample and the mica surfaces used for AFM imaging are hard to passivate, so only few reactions can take place on immobilized structures. This way it is only possible to run before-and-after experiments with rather large indicator molecules to detect the changes after the reaction has taken place (e.g. streptavidin or DNA hairpins).

These limitations need to be overcome on the way towards functional DNA nanostructures. A set of methods very well suited for the study of processes at very low concentration is provided by single-molecule fluorescence spectroscopy and microscopy. Small organic reporter molecules that are easily attached to a multitude of probes can be used to monitor spatial and/or spectral changes on the single-molecule level.

The study in associated publication P3 characterizes the fundamental dynamic process of binding and unbinding of fluorescently labeled DNA to an origami structure. Single stranded DNA with a covalently attached dye (imager strand) diffuses freely in solution while a DNA origami object attached to a glass surface contains the complementary strand (docking strand). The imager can now bind to the docking strand and thus generate a fluorescence signal on the surface. This binding event can be monitored on a TIRF microscope in real-time. The sequence of these strands is chosen such that it does not lead to a stable bond. As a result, the imager strand dissociates after a certain time, leaving the docking strand unoccupied and available for binding of another strand (figure 5.1). The kinetics of this reversible binding of DNA was quantified for different conditions (sequence length, strand concentrations, temperature). These were actually the first measurements that investigated DNA binding kinetics on the single molecule level with fluorescence microscopy.

Similar to a technique introduced by Sharonov and Hochstrasser in 2006 (PAINT)<sup>37</sup>, this reversible binding can also be exploited for super-resolution imaging (DNA-PAINT). Different origami structures were synthesized to demonstrate the applicability of DNA-PAINT and an optical resolution as low as 30 nm was achieved.

### 5.2 Possible applications of DNA-PAINT

#### 5.2.1 DNA-PAINT for the characterization of DNA origami

The study presented in P3 demonstrates the scope of using fluorescence for studying DNA nanostructures. The temporal information obtained is useful for the characterization of e.g. DNA or

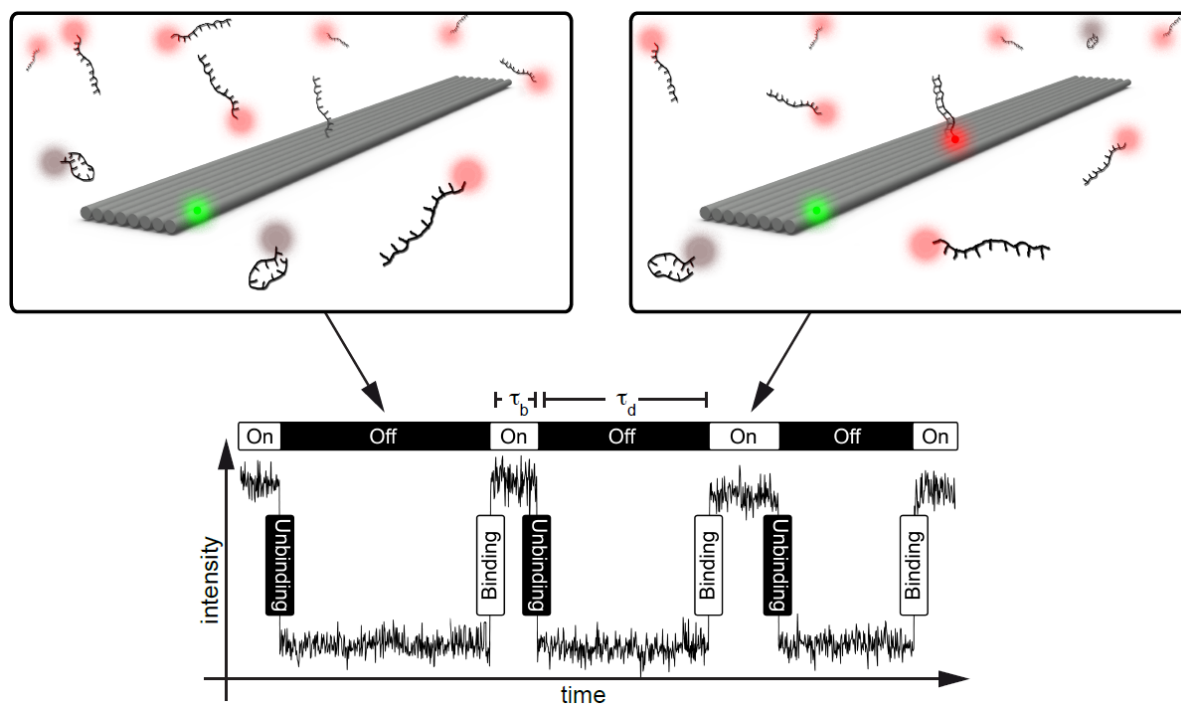


Figure 5.1: Schematic of DNA-PAINT. The two panels at the top show a DNA origami with and without imager strand attached. The bottom panel shows a typical fluorescence vs. time plot of DNA-PAINT<sup>36</sup>.

RNA detection systems<sup>38</sup>. The spatial information can be used to image the origami objects at sub-diffraction resolution and probe for the presence of individual staple strands in each structure. The latter becomes increasingly important for more complex assemblies. Although DNA origami fold correctly with a very high yield - as judged by AFM imaging - there is a finite probability of an individual staple strand not to be incorporated, so there is a need to probe the presence of each component that is needed to form a functional complex.

The particular advantage of DNA-PAINT for this purpose is its sequence specificity that enables probing for different targets. Furthermore, the label does not stay on the origami but is intrinsically removed and can easily be washed away. As mentioned in publication P3, photobleaching or inactive fluorophores do not corrupt the identification of docking sites.

### 5.2.2 DNA-PAINT imaging applied to cellular structures

Proof-of-principle experiments were also performed on cellular structures. This is particularly relevant as the study of many biological processes would profit from super-resolution imaging which is not limited by photobleaching. The main problem to overcome for cellular imaging is the labeling of the target structure with single stranded DNA.

This was achieved by an admittedly adventurous approach by the combination of a primary antibody, secondary antibody, neutravidin, and biotinylated DNA as depicted in figure 5.2. While this labeling strategy is certainly not optimal in terms of efficiency, stability and label size, it shows that super-resolution imaging of cellular structures is possible with DNA-PAINT. With improved labeling and fluorescent probes (increased quenching of unbound probes and minimal non-specific binding) this method is very promising to be widely applicable in biological imaging.

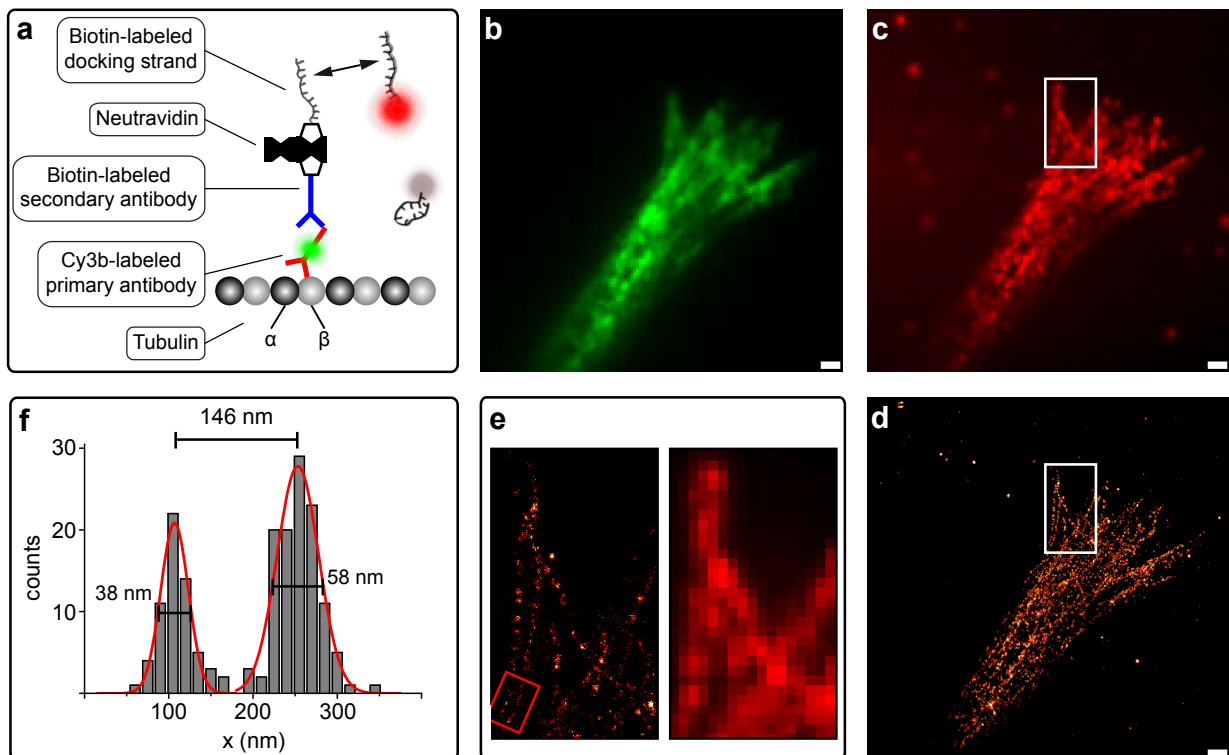


Figure 5.2: DNA-PAINT implemented for cellular imaging with antibodies exemplified by SR imaging of  $\beta$ -tubulin. a) Labeling strategy, b) conventional fluorescence image of Cy3 attached to the primary antibody, c) standard deviation image of DNA-PAINT with Atto655, d) SR reconstruction, e) zoom-in of marked region in c) and d), f) distance histogram of the region marked in e).

### 5.3 Associated Publication P3

## Single-Molecule Kinetics and Super-Resolution Microscopy by Fluorescence Imaging of Transient Binding on DNA Origami

By

R. Jungmann, C. Steinhauer, M. Scheible, A. Kuzyk, P. Tinnefeld and F.C. Simmel

published in

Nano Letters 10(11):4756-4761



# Four-Color Single-Molecule FRET Visualizes Energy Transfer Paths on DNA Origami.

By

I.H. Stein, C. Steinhauer and P. Tinnefeld

**Abstract:** Fluorescence resonance energy transfer represents a mechanism to transport light energy at the nano-scale as is exemplified by nature's light harvesting complexes. Here we used DNA origami to arrange fluorophores that transport excited state energy from an input dye to an output dye. We demonstrate that energy transfer paths can be controlled on the single-molecule level by the presence of a "jumper"-dye that directs the excited state energy either to a red or to an IR output dye. We used four-color single-molecule FRET with alternating laser excitation to sort subpopulations and to visualize the control of energy transfer.

submitted to

Journal of the American Chemical Society

## Bibliography

- [1] YuHuang Wang, Chad A Mirkin, and So-Jung Park. Nanofabrication beyond electronics. *ACS Nano*, 3(5):1049–1056, May 2009. doi: 10.1021/nn900448g. URL <http://dx.doi.org/10.1021/nn900448g>.
- [2] Web Reference:. Metamaterials for optical frequencies, 20.10.2010. URL <http://www.aph.kit.edu/wegener/?id=31>.
- [3] Héctor A Becerril and Adam T Woolley. DNA-templated nanofabrication. *Chem Soc Rev*, 38(2):329–337, Feb 2009. doi: 10.1039/b718440a. URL <http://dx.doi.org/10.1039/b718440a>.
- [4] Ernst Abbe. Beiträge zur Theorie des Mikroskops und der mikroskopischen Wahrnehmung. *Arch. Mikr. Anat.*, 9:413–468, 1873.
- [5] Jan Vogelsang, Christian Steinhauer, Carsten Forthmann, Ingo H Stein, Britta Person-Skegro, Thorben Cordes, and Philip Tinnefeld. Make them blink: probes for super-resolution microscopy. *Chemphyschem*, 11(12):2475–2490, Aug 2010. doi: 10.1002/cphc.201000189. URL <http://dx.doi.org/10.1002/cphc.201000189>.
- [6] Stefan W Hell. Far-field optical nanoscopy. *Science*, 316(5828):1153–1158, May 2007. doi: 10.1126/science.1137395. URL <http://dx.doi.org/10.1126/science.1137395>.
- [7] Michael J Rust, Mark Bates, and Xiaowei Zhuang. Sub-diffraction-limit imaging by stochastic optical reconstruction microscopy (STORM). *Nat Methods*, 3(10):793–795, Oct 2006. doi: 10.1038/nmeth929. URL <http://dx.doi.org/10.1038/nmeth929>.
- [8] Eric Betzig, George H Patterson, Rachid Sougrat, O. Wolf Lindwasser, Scott Olenych, Juan S Bonifacino, Michael W Davidson, Jennifer Lippincott-Schwartz, and Harald F Hess. Imaging intracellular fluorescent proteins at nanometer resolution. *Science*, 313(5793):1642–1645, Sep 2006. doi: 10.1126/science.1127344. URL <http://dx.doi.org/10.1126/science.1127344>.
- [9] M. G. Gustafsson. Surpassing the lateral resolution limit by a factor of two using structured illumination microscopy. *J Microsc*, 198(Pt 2):82–87, May 2000.
- [10] Russell E Thompson, Daniel R Larson, and Watt W Webb. Precise nanometer localization analysis for individual fluorescent probes. *Biophys J*, 82(5):2775–2783, May 2002. doi: 10.1016/S0006-3495(02)75618-X. URL [http://dx.doi.org/10.1016/S0006-3495\(02\)75618-X](http://dx.doi.org/10.1016/S0006-3495(02)75618-X).
- [11] Harry Nyquist. Certain topics in telegraph transmission theory. *Trans. Amer. Inst. Elect. Eng.*, 47, 1928.
- [12] Christian Steinhauer, Carsten Forthmann, Ralf Jungmann, Jan Vogelsang, Friedrich C Simmel, and Philip Tinnefeld. Nanoscopy using localization and temporal separation of fluorescence from single molecules. In B. D. Bartolo and J. Collins, editors, *Biophotonics: Spectroscopy, Imaging, Sensing, and Manipulation*, pages 87–106. Springer, 2011.

- [13] N. C. Seeman and N. R. Kallenbach. Design of immobile nucleic acid junctions. *Biophys J*, 44(2):201–209, Nov 1983. doi: 10.1016/S0006-3495(83)84292-1. URL [http://dx.doi.org/10.1016/S0006-3495\(83\)84292-1](http://dx.doi.org/10.1016/S0006-3495(83)84292-1).
- [14] Jung Huei Chen, Neville R. Kallenbach, and Nadrian C. Seeman. A specific quadrilateral synthesized from DNA branched junctions. *J Am Chem Soc*, 111(16):6402–6407, 1989.
- [15] N. C. Seeman. The use of branched DNA for nanoscale fabrication. *Nanotechnology*, 2:149–159, 1991.
- [16] Nadrian C Seeman. Nanomaterials based on DNA. *Annu Rev Biochem*, 79:65–87, 2010. doi: 10.1146/annurev-biochem-060308-102244. URL <http://dx.doi.org/10.1146/annurev-biochem-060308-102244>.
- [17] Paul W K Rothmund. Folding DNA to create nanoscale shapes and patterns. *Nature*, 440(7082):297–302, Mar 2006. doi: 10.1038/nature04586. URL <http://dx.doi.org/10.1038/nature04586>.
- [18] Shawn M Douglas, Hendrik Dietz, Tim Liedl, Björn Högberg, Franziska Graf, and William M Shih. Self-assembly of DNA into nanoscale three-dimensional shapes. *Nature*, 459(7245):414–418, May 2009. doi: 10.1038/nature08016.
- [19] Hendrik Dietz, Shawn M Douglas, and William M Shih. Folding DNA into twisted and curved nanoscale shapes. *Science*, 325(5941):725–730, Aug 2009. doi: 10.1126/science.1174251. URL <http://dx.doi.org/10.1126/science.1174251>.
- [20] Shawn M Douglas, Adam H Marblestone, Surat Teerapittayanon, Alejandro Vazquez, George M Church, and William M Shih. Rapid prototyping of 3d dna-origami shapes with cadnano. *Nucleic Acids Res*, 37(15):5001–5006, Aug 2009. doi: 10.1093/nar/gkp436. URL <http://dx.doi.org/10.1093/nar/gkp436>.
- [21] Mike Heilemann, Emmanuel Margeat, Robert Kasper, Markus Sauer, and Philip Tinnefeld. Carbocyanine dyes as efficient reversible single-molecule optical switch. *J Am Chem Soc*, 127(11):3801–3806, Mar 2005. doi: 10.1021/ja044686x. URL <http://dx.doi.org/10.1021/ja044686x>.
- [22] Graham T Dempsey, Mark Bates, Walter E Kowtoniuk, David R Liu, Roger Y Tsien, and Xiaowei Zhuang. Photoswitching mechanism of cyanine dyes. *J Am Chem Soc*, 131(51):18192–18193, Dec 2009. doi: 10.1021/ja904588g. URL <http://dx.doi.org/10.1021/ja904588g>.
- [23] Jonas Fölling, Mariano Bossi, Hannes Bock, Rebecca Medda, Christian A Wurm, Birka Hein, Stefan Jakobs, Christian Eggeling, and Stefan W Hell. Fluorescence nanoscopy by ground-state depletion and single-molecule return. *Nat Methods*, 5(11):943–945, Nov 2008. doi: 10.1038/nmeth.1257. URL <http://dx.doi.org/10.1038/nmeth.1257>.
- [24] Jan Vogelsang, Robert Kasper, Christian Steinhauer, Britta Person, Mike Heilemann, Markus Sauer, and Philip Tinnefeld. A reducing and oxidizing system minimizes photobleaching and blinking of fluorescent dyes. *Angew Chem Int Ed Engl*, 47(29):5465–5469, 2008. doi: 10.1002/anie.200801518. URL <http://dx.doi.org/10.1002/anie.200801518>.

- [25] Jan Vogelsang, Thorben Cordes, Carsten Forthmann, Christian Steinhauer, and Philip Tinnefeld. Controlling the fluorescence of ordinary oxazine dyes for single-molecule switching and superresolution microscopy. *Proc Natl Acad Sci U S A*, 106(20):8107–8112, May 2009. doi: 10.1073/pnas.0811875106. URL <http://dx.doi.org/10.1073/pnas.0811875106>.
- [26] Christian Steinhauer, Ralf Jungmann, Thomas L Sobey, Friedrich C Simmel, and Philip Tinnefeld. DNA origami as a nanoscopic ruler for super-resolution microscopy. *Angew Chem Int Ed Engl*, 48(47):8870–8873, 2009. doi: 10.1002/anie.200903308. URL <http://dx.doi.org/10.1002/anie.200903308>.
- [27] Thorben Cordes, Mathias Strackharn, Stefan W Stahl, Wolfram Summerer, Christian Steinhauer, Carsten Forthmann, Elias M Puchner, Jan Vogelsang, Hermann E Gaub, and Philip Tinnefeld. Resolving single-molecule assembled patterns with superresolution blink-microscopy. *Nano Lett*, 10(2):645–651, Feb 2010. doi: 10.1021/nl903730r. URL <http://dx.doi.org/10.1021/nl903730r>.
- [28] Alessandra Cambi, Frank de Lange, Noortje M van Maarseveen, Monique Nijhuis, Ben Joosten, Erik M H P van Dijk, Bärbel I de Bakker, Jack A M Fransen, Petra H M Bovee-Geurts, Frank N van Leeuwen, Niek F Van Hulst, and Carl G Figdor. Microdomains of the c-type lectin dc-sign are portals for virus entry into dendritic cells. *J Cell Biol*, 164(1):145–155, Jan 2004. doi: 10.1083/jcb.200306112. URL <http://dx.doi.org/10.1083/jcb.200306112>.
- [29] S. K. Kufer, E. M. Puchner, H. Gump, T. Liedl, and H. E. Gaub. Single-molecule cut-and-paste surface assembly. *Science*, 319(5863):594–596, Feb 2008. doi: 10.1126/science.1151424. URL <http://dx.doi.org/10.1126/science.1151424>.
- [30] Robert Kasper, Benjamin Harke, Carsten Forthmann, Philip Tinnefeld, Stefan W Hell, and Markus Sauer. Single-molecule STED microscopy with photostable organic fluorophores. *Small*, 6(13):1379–1384, Jul 2010. doi: 10.1002/smll.201000203. URL <http://dx.doi.org/10.1002/smll.201000203>.
- [31] Ramesh Subramani, Sissel Juul, Alexandru Rotaru, Felicie F Andersen, Kurt V Gothelf, Wael Mamdouh, Flemming Besenbacher, Mingdong Dong, and Birgitta R Knudsen. A novel secondary DNA binding site in human topoisomerase  $\alpha$  unravelled by using a 2D DNA origami platform. *ACS Nano*, 4(10):5969–5977, Oct 2010. doi: 10.1021/nn101662a. URL <http://dx.doi.org/10.1021/nn101662a>.
- [32] Zhao Zhang, Dongdong Zeng, Hongwei Ma, Guoying Feng, Jun Hu, Lin He, Can Li, and Chunhai Fan. A DNA-origami chip platform for label-free SNP genotyping using toehold-mediated strand displacement. *Small*, 6(17):1854–1858, Sep 2010. doi: 10.1002/smll.201000908. URL <http://dx.doi.org/10.1002/smll.201000908>.
- [33] Hongzhou Gu, Jie Chao, Shou-Jun Xiao, and Nadrian C Seeman. A proximity-based programmable DNA nanoscale assembly line. *Nature*, 465(7295):202–205, May 2010. doi: 10.1038/nature09026. URL <http://dx.doi.org/10.1038/nature09026>.

- 
- [34] Niels V Voigt, Thomas Tørring, Alexandru Rotaru, Mikkel F Jacobsen, Jens B Ravnsbaek, Ramesh Subramani, Wael Mamdouh, Jørgen Kjems, Andriy Mokhir, Flemming Besenbacher, and Kurt Vesterager Gothelf. Single-molecule chemical reactions on DNA origami. *Nat Nanotechnol*, 5(3):200–203, Mar 2010. doi: 10.1038/nnano.2010.5. URL <http://dx.doi.org/10.1038/nnano.2010.5>.
- [35] Masayuki Endo, Yousuke Katsuda, Kumi Hidaka, and Hiroshi Sugiyama. Regulation of DNA methylation using different tensions of double strands constructed in a defined dna nanostructure. *J Am Chem Soc*, 132(5):1592–1597, Feb 2010. doi: 10.1021/ja907649w. URL <http://dx.doi.org/10.1021/ja907649w>.
- [36] Ralf Jungmann, Christian Steinhauer, Max Scheible, Anton Kuzyk, Philip Tinnefeld, and Friedrich C Simmel. Single-molecule kinetics and super-resolution microscopy by fluorescence imaging of transient binding on dna origami. *Nano Lett*, Oct 2010. doi: 10.1021/nl103427w. URL <http://dx.doi.org/10.1021/nl103427w>.
- [37] Alexey Sharonov and Robin M Hochstrasser. Wide-field subdiffraction imaging by accumulated binding of diffusing probes. *Proc Natl Acad Sci U S A*, 103(50):18911–18916, Dec 2006. doi: 10.1073/pnas.0609643104. URL <http://dx.doi.org/10.1073/pnas.0609643104>.
- [38] Yonggang Ke, Stuart Lindsay, Yung Chang, Yan Liu, and Hao Yan. Self-assembled water-soluble nucleic acid probe tiles for label-free RNA hybridization assays. *Science*, 319:180–183, 2008.

## Acknowledgments

To GOD be the glory!

For the LORD gives wisdom, and from his mouth come knowledge and understanding.

I would like to thank all the people who made my time in Munich very enjoyable.

- First of all, Philip Tinnefeld for providing excellent supervision, for pinpointing the relevant questions and constantly being available for discussions. I had a great time in your group.
- Friedrich Simmel for being secondary advisor for the IDK-NBT, Tim Liedl for being second referee for this thesis, and Ken Jacobson for providing good biological samples as an application for SR experiments. I am very grateful to each of you for the good collaborations.
- Many thanks to Ralf for the many hours in and out of the lab, lots of good inspirations and teaching me to fold origami.
- Carsten helped me a lot with all the theory behind physics and with the setup of the microscope and the software.
- Thanks to Andi, Anton, Britta, Guillermo, Ingo, Jan, Martina, Max, Michelle, Moni, Philipp, Sarah, Sebastian, Tom, Thorben and Verena; all of you really contributed a lot to the success of this work.
- Thanks to Hermann Gaub and the Gambi Crew for all the support, discussions and infrastructure at the chair of applied physics.

I would also like to acknowledge the truly excellent research environment in Munich. People from the Center for NanoScience, the Nanosystems Initiative Munich and the Elite Network of Bavaria provided a lot of motivation, infrastructure and funding for my personal and scientific development.

I am also very grateful for the ongoing support of my parents and family.

Thank you Lydia, for everything.

Appendix

# Supporting Information

## Superresolution Microscopy on the Basis of Engineered Dark States

*Christian Steinhauer, Carsten Forthmann, Jan Vogelsang, Philip Tinnefeld\**

Angewandte Physik – Biophysik, and Center for NanoScience, Ludwig-Maximilians-Universität,  
Amalienstrasse 54, 80799 München (Germany)



Materials and methods, experimental details and results of simulations are provided in the supporting information.

### Microscope

Fluorescence imaging was performed on an Olympus IX-70 applying an objective-type total internal reflection fluorescence (TIRF) configuration with an oil-immersion objective (PlanApo N 60 $\times$ , NA 1.49, Olympus). The 647-nm and 531-nm lines of an Ar<sup>+</sup>Kr<sup>+</sup> laser (Stabilite 2018, Spectra Physics) were used for illumination. The laser beams were coupled into the microscope objective by a dual-band beamsplitter for 647 nm or 531 nm (Z647rdc, Dualband z532/633, AHF Analysentechnik). Fluorescence light was spectrally filtered with emission filters (HQ 700/75 M and BrightLine HC 582/75, AHF Analysentechnik) and imaged on an EMCCD camera (Andor Ixon DU-860D-CS0). Additional lenses were used to achieve a final imaging magnification of 200 fold, that is, a pixel size of 78 nm. Typical laser powers used for imaging were 80 mW (532 nm) and 140 mW (647 nm) yielding an excitation power density of  $\sim 18$  kW/cm<sup>2</sup>. The laser powers were chosen to adapt the on-times of the fluorophores to the shortest possible integration time of about 1 ms of the CCD-camera. Typically, we recorded 5000–10000 frames at frame rates of 1000 Hz.

Data shown in Figure 1 were collected with a confocal single-molecule setup described previously.<sup>1</sup> For confocal measurements, the laser beam of the Ar<sup>+</sup>Kr<sup>+</sup> laser was coupled into an oil immersion objective (UPLSAPO 60 $\times$ , NA 1.35, Olympus) by a dichroic beam splitter. The surface was scanned with a nano-positioning stage (P-527, Physik Instrumente) and the fluorescence was collected by the same objective and spatially filtered by a 50  $\mu$ m pinhole. The fluorescence signal was spectrally filtered using a band pass filter (HQ 700/75 M, AHF Analysentechnik) and the signal was imaged onto the active area of an avalanche photodiode (SPCM-AQRH-15, Perkin-Elmer). The setup is controlled by custom-made LabView software.

### Single molecule surfaces

LabTek 8-well chambered cover slides (Nunc) were treated with 0.1 % HF for 30 seconds and washed three times with PBS. They were then incubated with a solution of 3 mg/ml BSA and 0.6 mg/ml BSA/biotin (Sigma) in PBS for at least 4 hours at 4 °C. After washing three times with PBS, the surface was incubated with a  $\sim 0.1$  mg/ml solution of streptavidin for 5-10 min and washed again.  $\sim 10^{-9}$  M DNA solutions (IBA) were applied to the surface (Cy3B-DNA: single stranded: biotin-CGT AT(Cy3B)A GCT ATG CAA TATAAG TGT AAG GAA TCG AAT CGT A; Cy5-DNA: double stranded: Cy5-ATC GTT ACC AAA GCA TCG TAA TAG CAC GTT AAT TTA GCA CGG ACG ATC GCC-biotin) and washed three times with PBS.

For all experiments, oxygen was removed using an enzymatic oxygen-scavenging system, containing 10% (wt/vol) glucose, 10% (vol/vol) glycerol, 50  $\mu$ g/ml glucose oxidase, 100-200  $\mu$ g/ml catalase, and 0.1 mM Tris(2-carboxyethyl)phosphine hydrochloride (TCEP).

### Actin preparation

Actin filaments for in vitro experiments were polymerized from 5  $\mu$ M Alexa Fluor 647 conjugated actin monomers (Invitrogen) in a buffer containing 25 mM Imidazole, 25 mM KCl, 4 mM MgCl<sub>2</sub>, 1 mM EGTA and 1 mM DTT. After 5 min of polymerization, unlabeled phalloidin (Applichem) was added to a final concentration of 8  $\mu$ M to stabilize the filaments. The sample was immobilized on a glass surface coated with BSA and myosin (Sigma).

### Cell preparation

3T3 cells were plated in LabTek coverslide chambers. After 24-48 h, the cells were fixed using 3.7 % paraformaldehyde in PBS for 10 min. The fixed cells were washed three times with PBS and permeabilized in blocking buffer (PBS containing 5 % w/v bovine albumin serum (BSA; Sigma) and 0.5 % v/v Triton X-100) for 15 min. Cells were washed three times with PBS

containing 0.1 % v/v Tween 20 (Sigma). Microtubules were stained with mouse monoclonal anti- $\alpha$ -tubulin antibodies (Invitrogen) for 30 min and then with Alexa-647-labeled goat anti-mouse F(ab')<sub>2</sub> fragments (Invitrogen) serving as secondary antibodies, for 30 min. Three washing steps using PBS containing 0.1 % v/v Tween 20 were performed after each staining step. For “Blink Microscopy” oxygen was removed enzymatically and AA (500  $\mu$ M) was added.

### Data Analysis

**Intensity fluctuation analysis.** Autocorrelation analysis is employed to extract on- and off-times from single-molecule fluorescence intensity transients as described in the literature.<sup>2</sup>

The autocorrelation curve was fitted using a biexponential function. From this fit two amplitudes  $A_1$  and  $A_2$  and two characteristic times  $\tau_{ac1}$  and  $\tau_{ac2}$  were extracted. The first amplitude  $A_1$  and the first characteristic time  $\tau_{ac1}$  represent fast blinking of Cy5 due to cis-trans isomerization in the  $\mu$ s time regime and were neglected. For evaluating the on- and off-times in the ms time regime corresponding to the triplet and radical anion state, respectively, the on- and off-times were extracted from the background corrected second amplitude  $A_{2corr}$  and the second characteristic time  $\tau_{ac2}$  as follows:

$$\tau_{off} = \tau_{ac2} \cdot (1 + A_{2corr})$$

$$\tau_{on} = \tau_{ac2} \cdot \left(1 + \frac{1}{A_{2corr}}\right)$$

The background corrected amplitude  $A_{2corr}$  is determined from the experimental amplitude  $A_2$  by the following equation:

$$A_{2corr} = \left(\frac{S + B}{S}\right)^2 \cdot A_2$$

Here S corresponds to the average signal and B represents the background.

**Image reconstruction.** Movies were analysed by custom-made software written in LabView 7.1. Commonly the first 20 frames were discarded since in the beginning all molecules are in the active state and photodynamic equilibrium is achieved after about 20 frames with most molecules being prepared in the off-state. In some cases, when the fluorophore density was too high to resolve single emitters, the first up to 1500 frames were discarded. The spot finding routine involves a lower and upper threshold as well as a range for the size of the area above the lower threshold. However, in cases of high or inhomogeneous background a flexible threshold was used. In this algorithm the movie is analyzed frame by frame and each peak intensity within a frame is compared to its environment ( $7 \times 7$  pixels). When a certain contrast value is reached, the spot is considered for further analysis. Two-dimensional Gaussian fitting yields the position of the molecules that are histogrammed in 15-nm pixels for image reconstruction. To further exclude events with two molecules being simultaneously active within one diffraction limited area and to remove cases when the two-dimensional Gaussian fitting does not converge, a circularity criterion of the identified spots has to be met.

### “Blink Microscopy” of Single Molecules

Figure S1 shows total internal reflection images and the corresponding high resolution images of immobilized Cy5 (Figure S1a) and Cy3B (Figure S1b) molecules, respectively, recorded after enzymatic oxygen removal and addition of 100  $\mu$ M AA. Exploiting blinking, single molecules are clearly resolved in contrast to the diffraction limited wide-field image indicating the general applicability and multiplexing possibility.

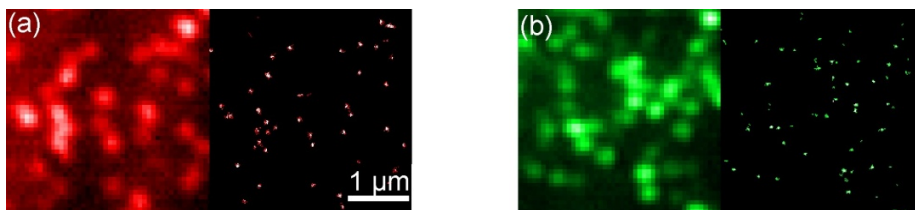


**Figure S1:** Total internal reflection (left) and “Blink Microscopy” (right) images of (a) single Cy5 labeled DNA molecules immobilized via streptavidin/biotin on BSA coated glass slides.

### Localization Precision

The localization precision is expected to be of the order of  $\sim s/(n^{1/2}) = 22$  nm where  $s$  represents the standard deviation of the point-spread-function. Experimentally, the localization precision was determined by repetitively localizing the same molecule for every on-state (Figure S2a). Accordingly, single molecules are localized with a standard deviation of  $s = 21$  nm (see Figure S2b). The slightly better localization precision in the experiments is due to the intensity threshold used for molecule identification, i.e. not all on-states are detected. Mechanical drift of the setup is negligible for the resulting total acquisition times of 1-10 s. This becomes also evident by the random distribution of localizations versus time (Figure S2c).

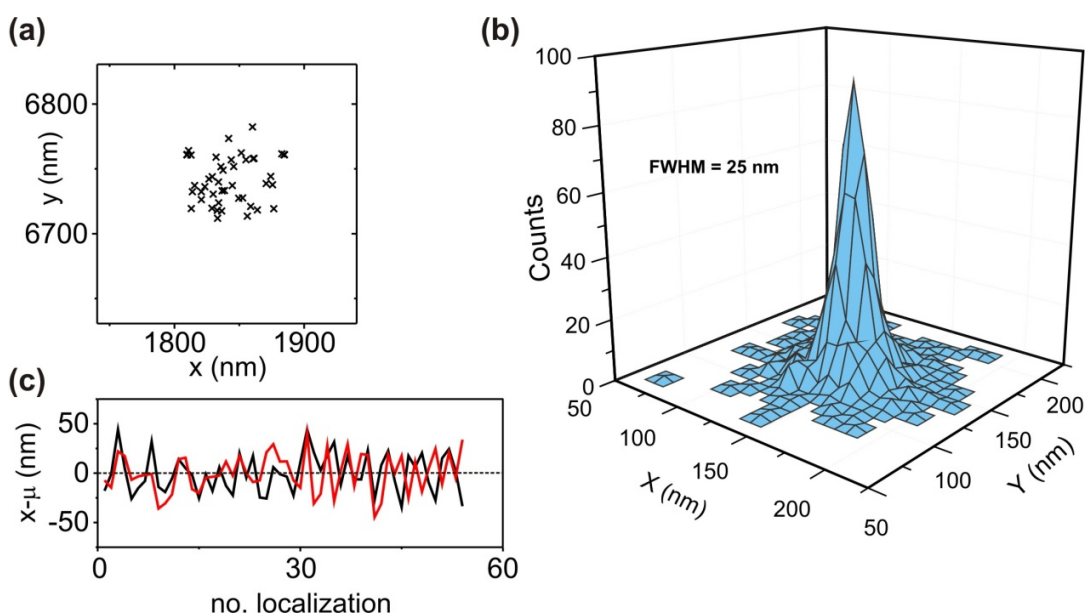


**Figure S2:** Localization precision of single molecules. (a) The centroid positions of the same molecule localized once for several on-times. (b) 2D-Histogram of many aligned localizations from single Cy5-DNA molecules demonstrates the localization precision with FWHM = 25 nm, i.e.  $s \sim 21$  nm. (c) The completely random distribution of localizations around the mean ( $\mu$ ) indicates the absence of drift during the time-scale of data acquisition ( $x$ - and  $y$ -values are represented in black and red, respectively).

### Simulations of “Blink Microscopy”

The resolution of subdiffraction-resolution microscopy using blinking molecules cannot be evaluated analytically. Among other factors, this is because two simultaneously emitting molecules do not necessarily deteriorate resolution. In many cases such two-molecule events are identified by the spot-finding algorithm either by the shape or by the intensity of the spot and excluded from further analysis. To theoretically analyse the resolution limit of “Blink Microscopy” under various conditions, we performed Monte Carlo simulations of single blinking

spots in a square grid. The simulated movies then undergo the same analysis procedure as the real data. We chose realistic parameters for the signal-to-noise ratio ( $S/N = 20$ , defined as the signal minus background divided by the standard deviation of the pixel-wise generated noise) and the number of cycles per molecule (100). Varied parameters are the distance of the molecules in the regular two-dimensional grid formed by the molecules (30 nm to 180 nm), and the ratio of off-time to on-time (on-times were kept constant and equal (however not synchronized) to data acquisition). The size of the grids was always of the order of the size of the PSF, so that it is effectively infinite.

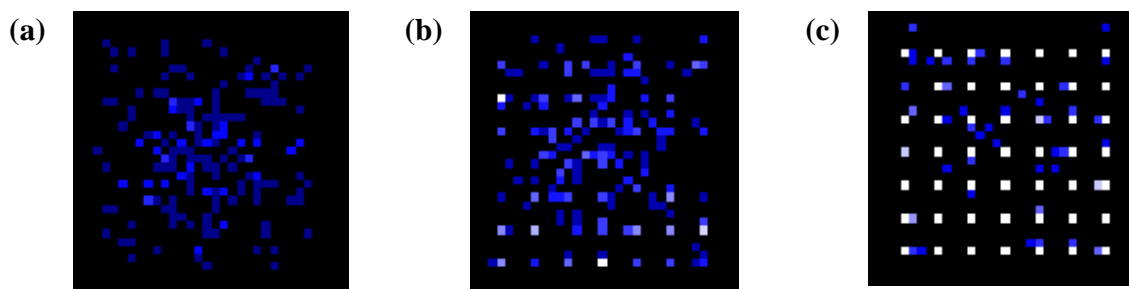


**Figure S3:** Three examples of simulated Blink Microscopy images of 60 nm grids for various  $\tau_{\text{off}}/\tau_{\text{on}}$  ratios. (a)  $\tau_{\text{off}}/\tau_{\text{on}} = 14$  (triplet-state-blinking) is clearly not sufficient to resolve the grid. (b)  $\tau_{\text{off}}/\tau_{\text{on}} = 30$ : the grid is resolved near the edges but not in the center. (c)  $\tau_{\text{off}}/\tau_{\text{on}} = 60$  (radical ion blinking) enables resolution of the grid structure.

Figure S3 shows three examples of simulations. A 60 nm grid is clearly not resolved using typical triplet blinking with  $\tau_{\text{off}}/\tau_{\text{on}} = 14$ . Almost resolvable is this grid with  $\tau_{\text{off}}/\tau_{\text{on}} = 30$ . Finally, with the typical anion lifetime of  $\tau_{\text{off}} = 60$  ms (on-state kept constant at 1 ms) this grid is clearly resolved. For the following discussion, a grid is defined as resolvable, if two specific points in the center are clearly separated (in analogy to Rayleigh’s criterion). Every condition was simulated 20 times and the fraction of resolvable grids was determined. Figure S4a shows this fraction as a function of the grid distance for seven  $\tau_{\text{off}}/\tau_{\text{on}}$  ratios (from left to right: 100, 60, 40, 30, 20, 14, 10). Taking the 50%-level of each of these curves gives a relation between the resolvable grid distance and the  $\tau_{\text{off}}/\tau_{\text{on}}$  ratio, shown in Figure S4b. The distance of points in the finest resolvable grid is stated as resolution in the manuscript. Accordingly the resolution of “Blink Microscopy” is  $<50$  nm for  $\tau_{\text{off}}/\tau_{\text{on}} = 60$  ms and  $\sim 100$  nm for  $\tau_{\text{off}}/\tau_{\text{on}} = 15$ .

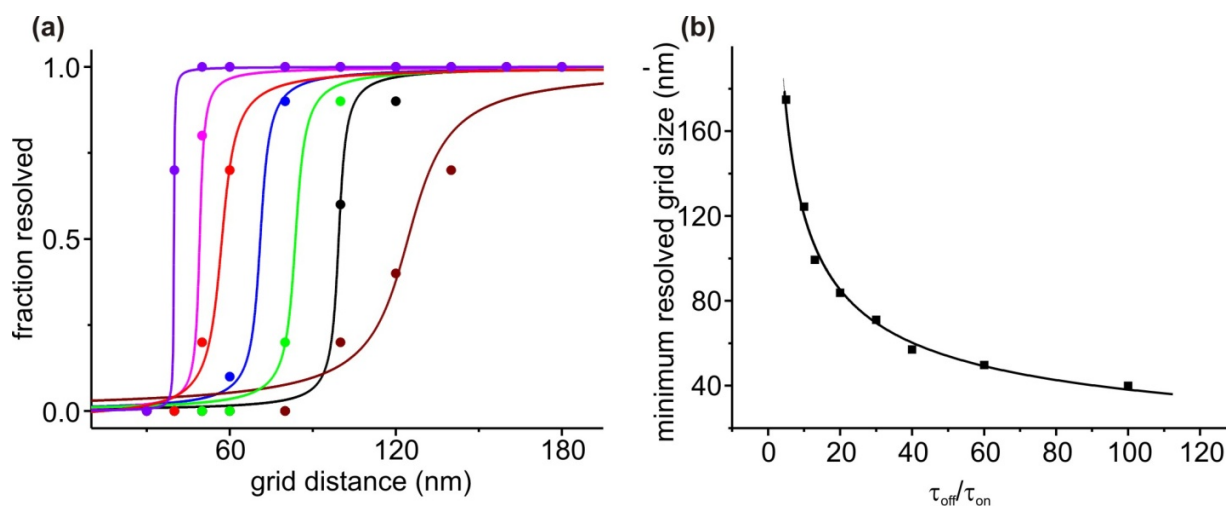


**Figure S4:** Analysis of simulations. (a) Fraction of grids which are resolvable as function of the grid distance for various  $\tau_{\text{off}}/\tau_{\text{on}}$  ratios (from left to right: 100, 60, 40, 30, 20, 14, 10). (b) Resolvable grid distance at a given  $\tau_{\text{off}}/\tau_{\text{on}}$  ratio.

---

Recently, however, it has been pointed out that not only the ability to measure the distance between two point-sources is defining resolution but that also the Nyquist criterion has to be met.<sup>3</sup> Accordingly, the sampling interval must be smaller than half the desired resolution. This means that for a resolved grid size of 50 nm the resolution is given by grid distance times two, that is 100 nm for  $\tau_{\text{off}}/\tau_{\text{on}} = 60$  (for redox-blinking Cy5 or Alexa 647 molecules). This so-called Nyquist limited resolution then is  $\sim 200$  nm for triplet blinking. To this end we have to mention that this calculation of resolution is not absolute but depends on the specific structure investigated and holds true only for a very regular grid. If more than one molecule is found per grid point the achievable resolution will decrease. Vice versa, if not all grid points are occupied by molecules (e.g. because a small and labelled structure is surrounded by a larger unlabeled structure), a better resolution can locally be achieved (as is the case at the edges of the grid in Figure S3b).

### References

- (1) Vogelsang, J.; Kasper, R.; Steinhauer, C.; Person, B.; Heilemann, M.; Sauer, M.; Tinnefeld, P. *Angew Chem Int Ed* **2008**, *47*, 5465-5469.
- (2) Yip, W. T.; Hu, D. H.; Yu, J.; Vanden Bout, D. A.; Barbara, P. F. *J. Phys. Chem. A* **1998**, *102*, 7564-7575.
- (3) Shroff, H.; Galbraith, C. G.; Galbraith, J. A.; Betzig, E. *Nat Methods* **2008**, *5*, 417-423.



## Supporting Information

© Wiley-VCH 2009

69451 Weinheim, Germany

---

DNA Origami as a Nanoscopic Ruler for Super-Resolution Microscopy  
*Christian Steinhauer<sup>+1</sup>, Ralf Jungmann<sup>+2</sup>, Thomas L. Sobey<sup>2</sup>, Friedrich C. Simmel<sup>\*2</sup>, Philip Tinnefeld<sup>\*1</sup>*

<sup>1</sup>Applied Physics – Biophysics & Center for NanoScience, Ludwig-Maximilians-Universität, Amalienstr. 54,  
D-80799 München, Germany

<sup>2</sup>Physics Department E14 & Center for NanoScience, Technische Universität München, James-Franck-Straße 1, D-85748  
Garching, Germany

<sup>+</sup> These authors contributed equally to this work.

<sup>\*</sup>To whom correspondence should be addressed:  
Email: philip.tinnefeld@lmu.de, [simmel@ph.tum.de](mailto:simmel@ph.tum.de)

## Experimental Section

### Sample Preparation

Unmodified staple strands were purchased from DNA Technology A/S (Risskov, Denmark) at a concentration of 150  $\mu\text{M}$  and were used without further purification. Fluorescently labeled and biotinylated staple strands were purchased PAGE purified from biomers.net (Ulm, Germany) at a concentration of 150  $\mu\text{M}$ . Microcon Centrifugal Filter Devices (100,000 MWCO) were purchased from Millipore (Billerica, USA). M13mp18 viral DNA (N4040S) was purchased from New England Biolabs, Inc. (Ipswich, USA).

The origami sample design is based on Rothmund's original rectangular design and the structures are formed with a molar ratio of 1:100 between the viral DNA and all the staple strands.<sup>[1]</sup> After the self-assembly by thermal annealing in a Thermocycler (Mastercycler® Personal, Eppendorf, Germany), the samples were purified using Microcon centrifugal filter devices (100,000 MWCO, 300 x g speed, 10 min) to remove excess staple strands.

### AFM Imaging

Samples were imaged in tapping mode using a Multimode V AFM with an E-scanner (Veeco Instruments, Santa Barbara, USA). Imaging was performed in TAE/Mg<sup>2+</sup> buffer solution with NP-S oxide-sharpened silicon nitride cantilevers (Veeco Probes, Camarillo, USA) using resonance frequencies between 7-9 kHz of the narrow 100  $\mu\text{m}$ , 0.38 N/m force constant cantilever.

After self-assembly of the origami structure  $\approx 20 \mu\text{l}$  of TAE/Mg<sup>2+</sup> buffer solution was dropped onto a freshly cleaved mica surface (Plano, Dresden, Germany) glued to a metal puck (Plano). After 30 s the mica surface was dried using a gentle stream of N<sub>2</sub> and 5  $\mu\text{l}$  of the origami solution was dropped onto the mica surface. After another 30 s, 30  $\mu\text{l}$  of additional buffer solution was added to the sample. Imaging parameters were optimized for best image quality while maintaining the highest possible setpoint to minimize damage to the samples. Images were post-processed by subtracting a 1st order polynomial from each scan line. Drive amplitudes were approximately 0.11 V, integral gains  $\sim 2$ , proportional gains  $\sim 4$ .

### Gel Electrophoresis

For gel electrophoresis 0.75 % Agarose (A9539, Sigma Aldrich, MO, USA) in 1x TAE buffer was heated to boiling and cooled to 50 °C and filled into the gel cask. Gel lanes were filled with 10  $\mu\text{l}$  of 1.6 pM M13mp18 scaffold, 10  $\mu\text{l}$  of unpurified origami structures, 10  $\mu\text{l}$  purified origami structures and 10  $\mu\text{l}$  excess staples. After running, the gel was stained with SYBR® Gold Nucleic Acid Gel Stain (Invitrogen, Carlsbad, CA, USA) and imaged with a custom-made gel documentation system.

### Immobilization Strategies

For non-specific adsorption to the glass surface, the cover glasses were incubated with 0.1 M hydrofluoric acid (HF) for 30 seconds and rinsed three times with PBS. Origami solution was applied directly to the glass slide and binding occurred upon addition of 1 M MgCl<sub>2</sub> to a final concentration of  $\sim 500 \text{ mM}$ . For all further measurements, the respective buffers were supplemented to contain 200 mM MgCl<sub>2</sub>.

For specific binding via biotin/streptavidin, the surface was treated with HF as described above. It was then incubated with 1 mg/ml bovine serum albumin (BSA) and 0.2 mg/ml biotin labeled BSA (Sigma) for 3-4 hours. After three washing steps with PBS, surfaces were incubated with 0.2 mg/ml streptavidin (IBA, Germany) for 10-20 minutes and washed again.

### Fluorescence Microscopy

All fluorescence imaging was carried out on an inverted microscope Olympus IX-71 applying an objective-type total internal reflection fluorescence (TIRF) configuration with an oil-immersion objective (UPlanSApo 100X, NA 1.40 Oil, Olympus). Additional lenses were used to achieve a final imaging magnification of  $\sim 160$  fold, corresponding to a pixel size of 137 nm. Samples were imaged using microscopic chamber slides (LabTek, Nunc).

For illumination, a high power single mode diode laser ( $\lambda=650 \text{ nm}$ , XTL, Toptica) was used, illuminating an area of about twice the size of the observation area ( $\sim 600 \mu\text{m}^2$ ).

The laser beam was filtered with a clean up filter (Brightline HC 650/13, AHF Analysentechnik) and coupled into the microscope objective by a dual-band beamsplitter (z532/658rpc, AHF Analysentechnik).

Fluorescence light was spectrally filtered with an emission filter (HQ 700/75 M, AHF Analysentechnik) and imaged on an EMCCD camera (Andor Ixon DU-860D-CS0). For dSTORM measurements, an additional filter was placed in the detection path (Razoredge Long Pass 568, AHF Analysentechnik) to efficiently block the additional 532 nm laser (Rapidus, Compact Laser Solutions, Germany). The green light required for switching of Cy5 is overlaid with the red laser beam by a dichroic mirror (600DCXR, AHF Analysentechnik).

### Blink Microscopy

DNA Origami structures labeled with ATTO655 were immobilized to the glass in PBS containing 50  $\mu\text{M}$  ascorbic acid and 50-100  $\mu\text{M}$  N,N-methylviologen (MV). MV concentration was adjusted to gain sufficient localizations within 20 seconds to avoid mechanical drift (see ref. <sup>[2]</sup> for details of how to adjust blinking for super-resolution microscopy). The typical laser power used for imaging was 200 mW. 2000-4000 frames were recorded at frame rates of 150-250 Hz. Under these conditions, ATTO 655 emits approx. 1000 photons per ON-time.



---

## **dSTORM**

For dSTORM measurements, oxygen was removed using the enzymatic glucose-oxidase oxygen scavenging system.<sup>[3]</sup> The LabTek chamber is filled with PBS containing 10% (wt/vol) glucose and 10% (vol/vol) glycerol. Directly before the measurement, 2-mercaptoethylamine (MEA) is added to a concentration of 50 mM and oxygen removal is initiated with 50 µg/mL glucose-oxidase (Sigma) and 100 µg/mL catalase (Sigma). Excitation powers were 17 mW at 650 nm and 8 mW at 532 nm.<sup>[4]</sup> The recording time was 200 s at 10 Hz.

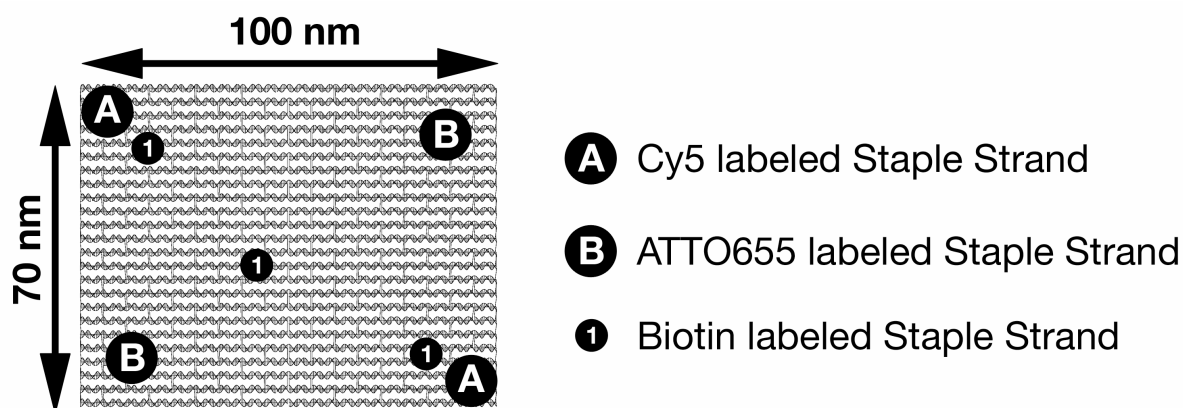
## **Photobleaching**

Photobleaching experiments on ATTO 655 were performed in PBS. 1000-2000 frames were recorded with an integration time of 100 ms or until all fluorophores were bleached.

## **Sample Design and DNA Sequences**

All names for the staple strands in the following chapter correspond to the ones used for the rectangle<sup>[1]</sup>. For Cy5 labeling, staple strands r-7t2f and r7t22e (position marked with A in Scheme S1) were extended with 4 thymine bases on the 5' end and labeled with a Cy5 fluorophore at that end. The same procedure was applied for the ATTO 655 labeled staples r-7t20f and r7t4e (position marked with B in Scheme S1).

Biotinylated staple strands (marked with 1 in Scheme S1) were designed by splitting and merging of two adjacent strands such that the resulting 5' end is shifted by three half-turns compared to the 5' end of the unmodified strands. By this it is ensured that the biotin label is located on the opposite side of the origami compared to the fluorophore positions. All modified staple strands and their sequences are given in Table S4.



**Scheme S1:** Cy5 and ATTO 655 modified staple strands are located at positions marked with A and B on the origami respectively. Their theoretical distance is 99.1 nm for Cy5 and 89.5 nm for ATTO 655 modified staples. Biotinylated staple strands are located at positions highlighted with 1 and protrude to the opposite side of the origami structure by design.

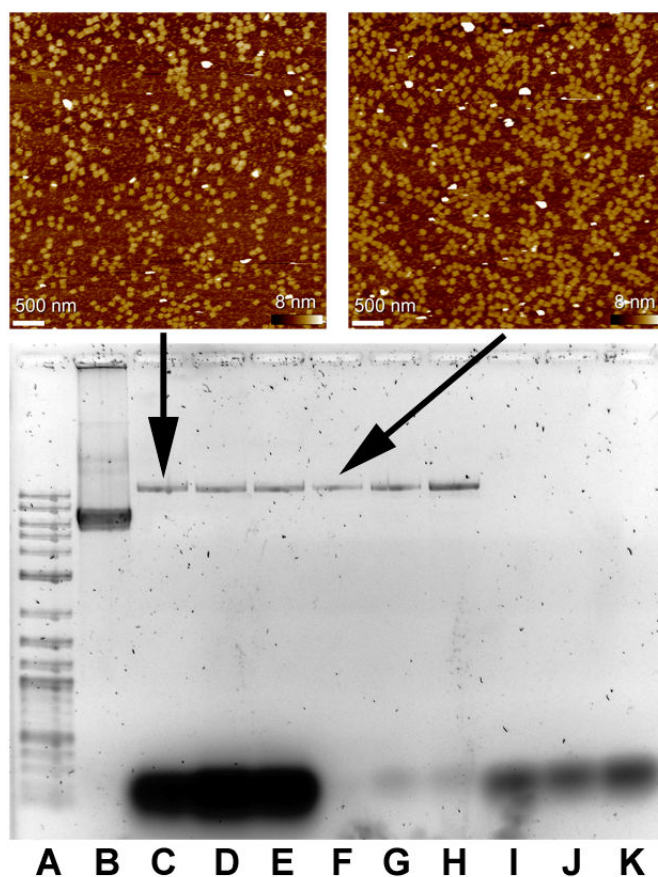


**Figure S1:** AFM and gel electrophoresis images of purified and unpurified DNA origami samples. **Top:** AFM image on the left shows the rectangular structures before filtering, on the right after filtering. **Bottom:** Agarose gel electrophoresis showing origami structures along with a DNA 2log ladder, the M13mp18 scaffold and the staples before and after filtering. Lanes on the right show the excess staples, which were filtered out. (A) 2log ladder, (B) M13mp18 scaffold strand, (C-E) unpurified origami samples showing folded structures and excess staples, (F-H) purified origami samples, (I-K) excess staples.

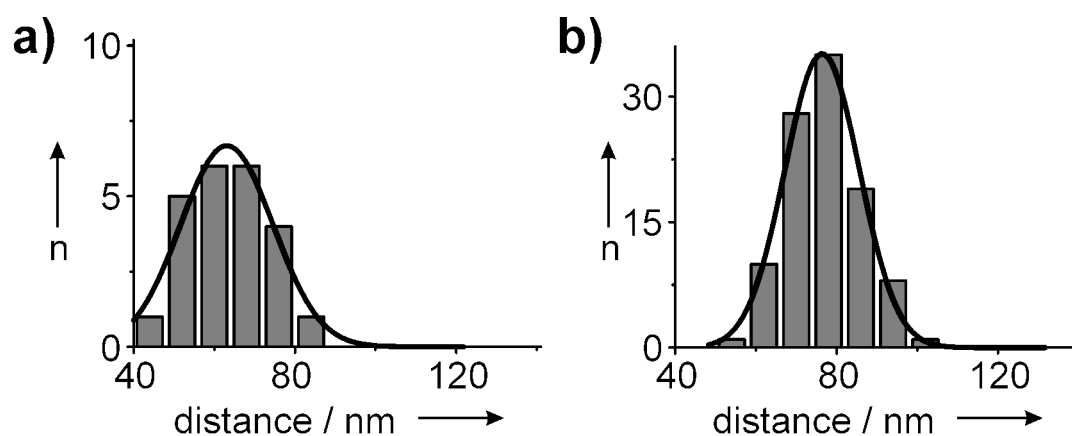


**Figure S2:** Distance distribution histograms of DNA-origami labeled with two ATTO655 immobilized via a) one and b) three biotin linkers.

**Table S4:** Modified staple strands used in this work: The unmodified staple strand sequences from Rothemund's original design<sup>[1]</sup> are given in the left column. Modified strand sequences are shown on the right. A biotinylated strand is designed by merging the region marked in red from r-5t4f and the region marked in green from r-5t6f. In addition a 4 thymine bases long spacer region is added on the 5' end and the strand is labeled on that end. Staples labeled with fluorophores are extended with 4 thymine bases on the 5' end and labeled on that end with Cy5 or ATTO 655. Base sequence direction is from 5' to 3'.

Unmodified Strand	Modified Strand
r-5t4f, TTTCATGAAAATTGTGTCGAAATCTGTACAGA	Biotin-TTTTTCGAAATCTGTACAGACCAGGCGCTTAATCAT
r-5t6f, CCAGGCGCTTAATCATTGTGAATTACAGGTAG	
r5t18f, GCGCAGAGATATCAAAATTATTGACATTATC	Biotin-TTTTTATTATTGACATTATCATTTTGCGTCTTAGG
r5t20f, ATTTTGCGTCTTAGGAGCACTAAGCAACAGT	
r-1t14f, AGGTAAAGAAATCACCATCAATATAATATTTT	Biotin-TTTTCATCAATATAATATTTTGTAAAATTTTAACC
r-1t16f, GTTAAAATTTTAACCAATAGGAACCCGGCACC	
r-7t2f, GAGAATAGCTTTTGCGGGATCGTCGGGTAGCA	Cy5-TTTTGAGAATAGCTTTTGCGGGATCGTCGGGTAGCA
r7t22e, GCCAACAGTCACCTTGCTGAACCTGTTGGCAA	Cy5-TTTTGCCAACAGTCACCTTGCTGAACCTGTTGGCAA
r-7t20f, CTTGCATGCATTAATGAATCGGCCCGCCAGGG	ATTO655-TTTTCTTGCATGCATTAATGAATCGGCCCGCCAGGG
r7t4e, TGCCTTTAGTCAGACGATTGGCCTGCCAGAAT	ATTO655-TTTTGCCTTTAGTCAGACGATTGGCCTGCCAGAAT

## References

- [1] P. W. Rothemund, *Nature* **2006**, *440*, 297.
- [2] J. Vogelsang, T. Cordes, C. Forthmann, C. Steinhauer, P. Tinnefeld, *Proc Natl Acad Sci U S A* **2009**, *106*, 8107.
- [3] T. Ha, I. Rasnik, W. Cheng, H. P. Babcock, G. H. Gauss, T. M. Lohman, S. Chu, *Nature* **2002**, *419*, 638.
- [4] M. Heilemann, S. van de Linde, M. Schuttelpelz, R. Kasper, B. Seefeldt, A. Mukherjee, P. Tinnefeld, M. Sauer, *Angew Chem Int Ed Engl* **2008**, *47*, 6172.

## Supporting Information

# Single-molecule kinetics and super-resolution microscopy by fluorescence imaging of transient binding on DNA origami

Ralf Jungmann, Christian Steinhauer, Max Scheible, Anton Kuzyk, Philip Tinnefeld, and Friedrich C. Simmel

## Materials and Methods

### DNA origami design

LRO monomers and oligomers were designed using caDNAnanoSQ 0.2.3<sup>1</sup>. Details of the design can be found in Figure S9, DNA sequences are listed in Table S10 and S11 for the LRO and RRO structures respectively. Splitting of two adjacent staple strands and joining the last 16 nt of one staple to the first 16 nt of the following staple creates a strand whose 5'-end is pointing in an opposite direction (e.g. "downwards") compared to the rest of the staple strands (for more detailed information see Steinhauer et al.<sup>2</sup>). In addition, a spacer region composed of four thymidines is added to the 5'-end and the strand is labeled with biotin on that end. These strands are used to immobilize the origami structures to a BSA/biotin/streptavidin glass surface.

### Sample preparation

Unmodified staple strands were purchased from Bioneer Inc. (Alameda, USA) and DNA Technology A/S (Risskov, Denmark) and were used without further purification. PAGE purified staple strands labeled with fluorophores or biotin were purchased from biomers.net (Ulm, Germany) and IBA (Göttingen, Germany). Amicon Ultra Centrifugal Filter Devices (100,000 MWCO) were purchased from Millipore (Billerica, USA). M13mp18 viral DNA (N4040S) was purchased from New England Biolabs, Inc. (Ipswich, USA). The origami structures were formed with a molar ratio of 1:10 between the viral DNA and all the staple strands. After the self-assembly by thermal annealing in a thermocycler (Mastercycler Personal, Eppendorf, Germany), the samples were purified twice using Amicon Ultra centrifugal filter devices (100,000 MWCO, 14000 x g speed, 5 min) to remove excess staple strands.

---

For specific binding via biotin/streptavidin, a chambered cover glass slide (LabTek, NUNC, USA) was treated with 0.1 M hydrofluoric acid (HF) for 30 seconds and rinsed three times with phosphate buffered saline (PBS). It was then incubated with 1 mg/ml bovine serum albumin (BSA) and 0.2 mg/ml biotin labeled BSA (Sigma) for 3–4 hours. After three washing steps with PBS, surfaces were incubated with 0.2 mg/ml streptavidin (IBA, Germany) for 10–20 minutes and washed again. 2–10  $\mu$ l of purified origami solution was diluted in 50  $\mu$ l 1 M  $MgCl_2$  and applied directly onto the glass surface until sufficient molecules were bound. As imaging buffer solution 1 x PBS containing altogether 600 mM NaCl was used.

### **AFM imaging and image analysis**

Samples were imaged using tapping or peak force tapping mode on a Multimode VIII AFM with an E-scanner (Veeco Instruments, Santa Barbara, USA). Imaging was performed in TAE/ $Mg^{2+}$  buffer solution with DNP-S oxide-sharpened silicon nitride cantilevers and SNL sharp nitride levers (Veeco Probes, Camarillo, USA) using resonance frequencies between 7-9 kHz of the narrow 100  $\mu$ m, 0.38 N/m force constant cantilever. After self-assembly of the origami structure  $\approx$  20  $\mu$ l of TAE/ $Mg^{2+}$  buffer solution was deposited onto a freshly cleaved mica surface (Plano, Dresden, Germany) glued to a metal puck (Plano). After 30 s the mica surface was dried using a gentle stream of  $N_2$  and 5  $\mu$ l of the origami solution was deposited onto the mica surface. After another 30 s, 30  $\mu$ l of additional buffer solution was added to the sample. Imaging parameters were optimized for best image quality while maintaining the highest possible set point to minimize damage to the samples. Images were post-processed by subtracting a 1<sup>st</sup> order polynomial from each scan line. Drive amplitudes were approximately 0.11 V, integral gains  $\approx$  2, proportional gains  $\approx$  4.

AFM image analysis for length and angular distribution was performed using custom-written LabVIEW (National Instruments, Austin, USA) software.

### **Fluorescence microscopy imaging and fluorescence spectroscopy**

Fluorescence imaging was carried out on an inverted microscope Olympus IX-71 (Olympus Corporation, Japan) applying an objective-type total internal reflection fluorescence (TIRF) configuration with an oil-immersion objective (UPlanSApo 100X, NA 1.40 Oil, Olympus). Additional lenses were used to achieve a final imaging magnification of  $\sim$ 160 fold, corresponding to a pixel size of 145 nm. Samples were imaged using

microscopic chamber slides (LabTek, Nunc). For ATTO655 imaging, a high power single mode diode laser ( $\lambda=650$  nm, XTL, Toptica) was used, illuminating an area of about twice the size of the observation area ( $\sim 600 \mu\text{m}^2$ ). The laser beam was filtered with a clean up filter (Brightline HC 650/13, AHF Analysentechnik) and coupled into the microscope objective by a dual-band beamsplitter (z532/658rpc, AHF Analysentechnik). Cy3b was excited with a 532 nm DPSS laser (Rapidus, Compact Laser Solutions, Germany). Fluorescence light was spectrally filtered with an emission filter (HQ 700/75 M or BrightLine HC 582/75, AHF Analysentechnik) and imaged on an EMCCD camera (Andor Ixon DU-897). The sample temperature was adjusted by cooling/heating the objective with a digitally controlled water bath (VWR, Germany).

For kinetic measurements as well as DNA-PAINT imaging typically 5000 frames were recorded at a frame rate of 10 Hz. The laser intensity was set as low as possible to avoid photobleaching while being sufficiently high to obtain a reasonable signal-to-background ratio, which was in the range of 4–8 mW. To exclude effects of photobleaching from kinetics measurements,  $\tau_b$  was measured at a fixed position for different excitation intensities. Significant photobleaching effects could only be observed at laser powers  $> 100$  mW (data not shown).

To obtain reliable data from kinetics measurements, for each data point usually 5 positions of the sample chamber were analyzed. Each data point represents the average of 200–500 origami structures where 50–100 molecules were found in each movie.

Fluorescence spectrometry measurements for guanine induced quenching of ATTO655 in solution was carried out on a Fluoromax-3 fluorescence spectrometer (Horiba Jobin-Yvon, USA) at an excitation wavelength of 650 nm.

### **Data analysis**

Super-resolution images were reconstructed from the raw data based on 2-dimensional Gaussian fitting with a custom made LabVIEW program<sup>3</sup>. A simplified version of this software is available for download at [www.e14.ph.tum.de](http://www.e14.ph.tum.de). Kinetic information is also extracted with LabVIEW software. In each frame, the algorithm identifies peak intensity pixels and compares them to their local environment ( $8 \times 8$  pixels). When a certain contrast value is reached, the pixel is considered to be “on”. All such pixels that are in direct contact are combined in spots, which are interpreted to be diffraction-limited representations of fluorescently labeled DNA bound on a DNA origami structure. The superposition of all spots yields a 2-dimensional mask that is used to generate binary

binding profiles for each origami structure. For each binding profile the on and off-times of each binding event are extracted. ON and OFF-times are summarized in an array for each experimental condition e.g. different imager strand concentrations. Average ON and OFF-times are obtained by fitting a single exponential function  $P = 1 - e^{-t/\tau}$  to the binding/unbinding probability  $P_{\text{bound}}$  and  $P_{\text{unbound}}$ , respectively<sup>4</sup>.

Diffraction-limited imaging with DNA-PAINT is performed by recording an image stack consisting of 5000 frames; this stack is then divided in four sub-stacks, each containing 1250 frames. On each sub-stack a standard-deviation z-projection is carried out resulting in one single frame. Subsequently these four standard-deviation frames are subjected to a mathematical operation resulting in the smallest pixel-value between all four frames. This operation – together with the standard-deviation projection – robustly rules out non-specific fluorescence signals (cf. Figure S2).

### Estimation of unbinding rates

The “off” rate for unbinding of an imager strand from a docking strand is approximately exponentially dependent on the length of the duplex. This can be easily seen when treating the dissociation process as a random walk with a reflecting and an absorbing boundary. For short DNA duplexes of length  $n$  dissociation starts from the ends, where thermal fluctuations lead to the breaking of terminal base-pairs (“fraying”). After the first bp is broken, it may either reform or the adjacent bp may also break, and so on. The duplex is assumed to completely dissociate, when a critical duplex length, e.g.  $N=3$ , is reached. The mean first passage time for this random process is approximately given by  $t \approx s^{n-N} \cdot (2k_+(n-N))^{-1}$  leading to a dissociation rate of  $k_{\text{off}} \approx 2k_+(n-N)s^{-(n-N)}$  (Ref. 5). Here,  $s$  denotes the stability constant for one base-pair:  $s = k_+/k_- = \exp(-\Delta G_{bp}/k_B T)$ , and  $k_+$  and  $k_-$  are rates for the formation and breaking of a single base-pair. For typical values of  $-\Delta G_{bp} \approx 3k_B T$  and  $k_+ = 10^7 \text{ s}^{-1}$  the off-rates are on the order of  $1.8 \text{ s}^{-1}$  and  $0.11 \text{ s}^{-1}$  for 9 and 10 bp duplexes, respectively. This is in remarkable agreement with our experimental results.

## Resolution

Without instrument drift and mechanical fluctuations of the imager/docking duplex, the resolution of the SR technique could be extremely high. When using very photostable fluorescent probes like quantum dots or ROXS stabilized organic fluorophores<sup>6</sup>. ATTO647N for example can emit 12 million photons on average before it bleaches. When background noise is omitted by choosing near-zero concentrations, a theoretical resolution of 1 Å could be achieved ( $d_{\min} = FWHM/\sqrt{n}$ , with n: number of emitted photons and FWHM: width of PSF).

## Efficiency

To investigate the imaging efficiency of DNA-PAINT – i.e. how many existing docking strands on DNA origami could be imaged – we carried out a combination of AFM and fluorescence measurements. First, RROs were prepared as described before using a 10 x excess of staple strands over the scaffold strand. After formation and purification, streptavidin was added to the origami solution in 100 x as well as 200 x excess. The two concentrations of streptavidin were used to make sure that the solution was saturated. No difference in binding efficiency was found for 100 x and 200 x excess of streptavidin. After several hours of incubation, origamis were transferred to a mica surface and imaged with an AFM in liquid. From the acquired images, the number of double and triple-“labeled” origami structures was counted (cf. Figure S8a).

Using DNA-PAINT, we also counted the number of double and triple-“labeled” structures. The result is shown in Figure S9a.



## Supplementary Figures and Tables

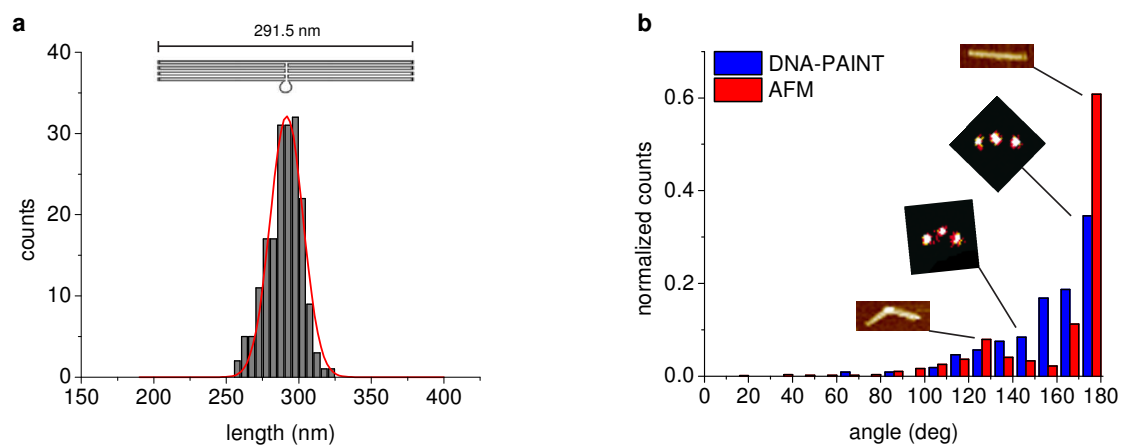


**Figure S1:** **a**, Length distribution of LRO monomers determined by AFM: designed length is 291.5 nm, measured length is  $290 \pm 10$  nm. **b**, Angular distribution of LRO monomers obtained by analysis of DNA-PAINT and AFM images respectively ( $n_{\text{DNA-PAINT}} = 107$ ,  $n_{\text{AFM}} = 854$ ). The angle is defined between three points in the DNA-PAINT images and two lines in the AFM images.

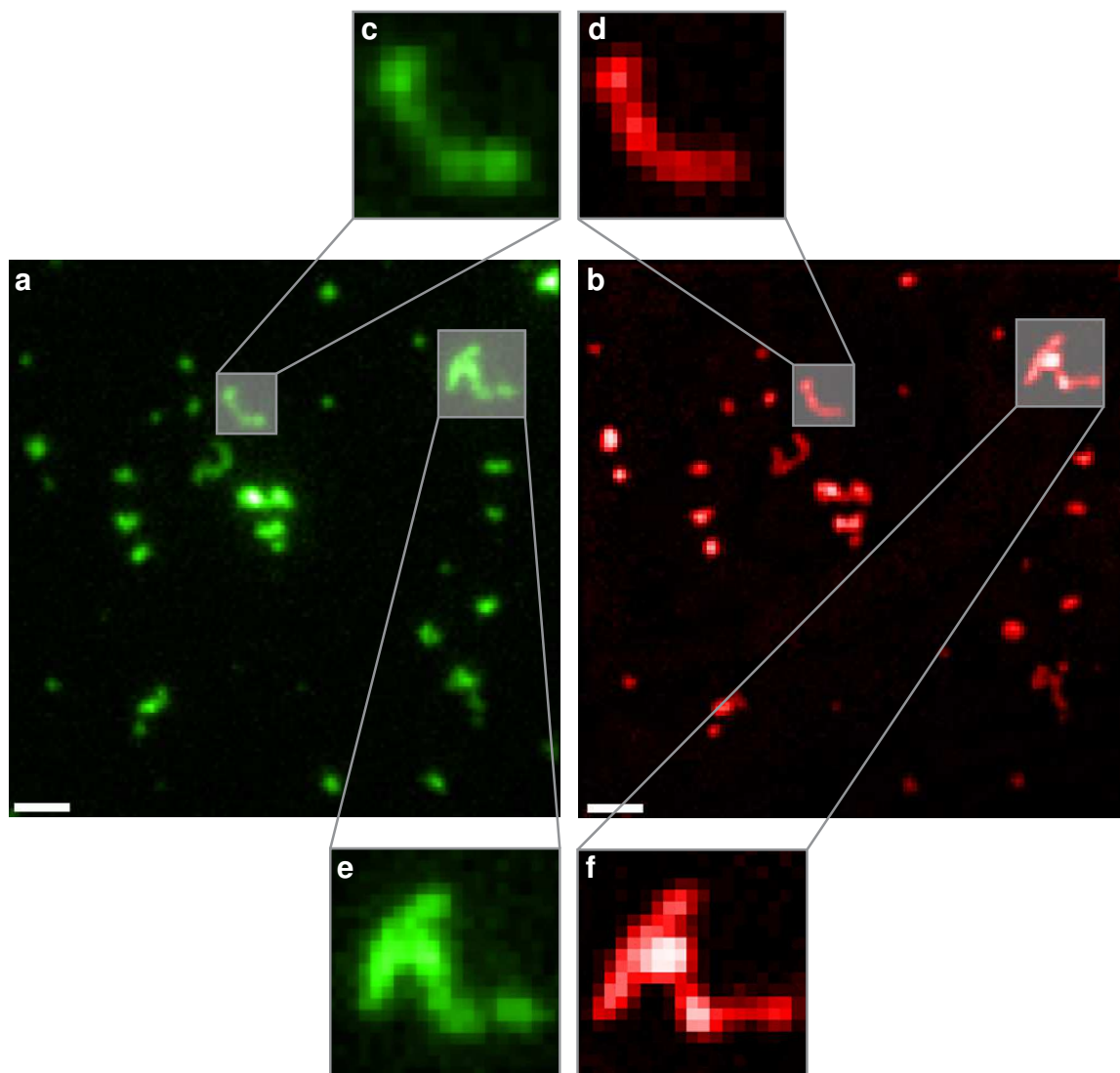


**Figure S2:** **a, c, e**, Diffraction-limited TIRF imaging of LRO oligomers labeled with ATTO532. Images are obtained by accumulating 20 frames. **b, d, f**, Diffraction-limited TIRF imaging of the same ROI using DNA-PAINT. Images are obtained by calculating the standard deviation image from 5000 frames. Length scale: 1.7  $\mu\text{m}$ . **c, d** and **e, f** are enlarged sections of **a** and **b** respectively.

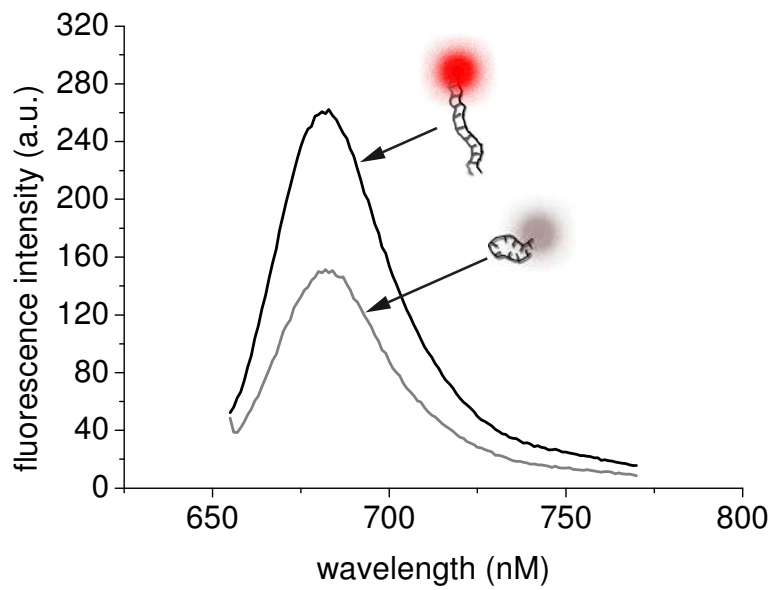


**Figure S3:** Quenching of ATTO655 fluorescence emission in solution. The single stranded DNA-PAINT imager strand labeled with ATTO655 shows reduced fluorescence in its entangled state due to quenching by the DNA base guanine in close proximity (grey curve). Upon binding to its complement (e.g. on the surface of a DNA origami), the DNA-PAINT imager strand is stretched and the mean distance to guanine in the base sequence increases, leading to an approximate 70 % increase in fluorescence intensity. This – acting in concert with TIRF illumination – leads to an enhanced signal-to-noise ratio of the fluorescence of imager strands bound in a duplex compared to background fluorescence from diffusing strands in solution.

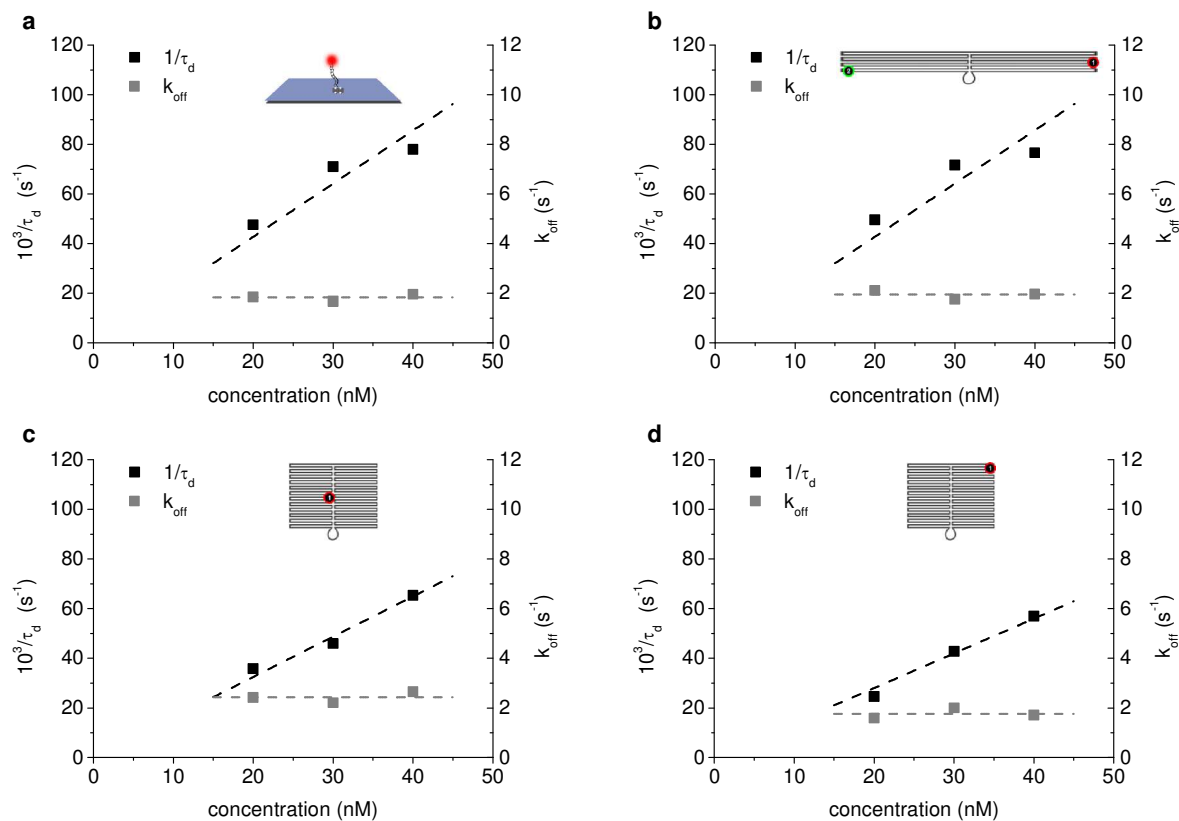


**Figure S4: a-d**, Kinetic analysis of DNA binding and unbinding kinetics using DNA-PAINT for different samples and sites. **a**, Surface immobilized 9bp DNA-PAINT docking strand (on a glass slide without DNA origami):  $k_{on} = 2.2 \cdot 10^6 \text{ M}^{-1}\text{s}^{-1}$ ,  $k_{off} = 1.8 \text{ s}^{-1}$ . **b**, DNA-PAINT docking strand on an LR origami structure at an edge position:  $k_{on} = 2.2 \cdot 10^6 \text{ M}^{-1}\text{s}^{-1}$ ,  $k_{off} = 1.7 \text{ s}^{-1}$ . **c**, DNA-PAINT docking strand on an RR origami at a center position:  $k_{on} = 1.6 \cdot 10^6 \text{ M}^{-1}\text{s}^{-1}$ ,  $k_{off} = 2.4 \text{ s}^{-1}$ . **d**, DNA-PAINT docking strand on an RR origami at an edge position:  $k_{on} = 1.4 \cdot 10^6 \text{ M}^{-1}\text{s}^{-1}$ ,  $k_{off} = 1.7 \text{ s}^{-1}$ .

**Table S5:** DNA hybridization constants for a 9 nt long imager strand determined by kinetic analysis using DNA-PAINT for LR origami center and edge site, RR origami center and edge site as well as a control docking strand immobilized on a glass surface.

	LRO center	LRO edge	RRO center	RRO edge	Surface
$k_{on}$ ( $10^6$ (Ms) $^{-1}$ )	$2.3 \pm 0.1$	$2.2 \pm 0.2$	$1.6 \pm 0.1$	$1.4 \pm 0.1$	$2.2 \pm 0.2$
$k_{off}$ ( $s^{-1}$ )	$1.6 \pm 0.2$	$1.7 \pm 0.2$	$2.4 \pm 0.2$	$1.7 \pm 0.2$	$1.8 \pm 0.1$
$K_d$ ( $\mu$ M)	$0.7 \pm 0.1$	$0.8 \pm 0.2$	$1.5 \pm 0.2$	$1.2 \pm 0.2$	$0.8 \pm 0.1$

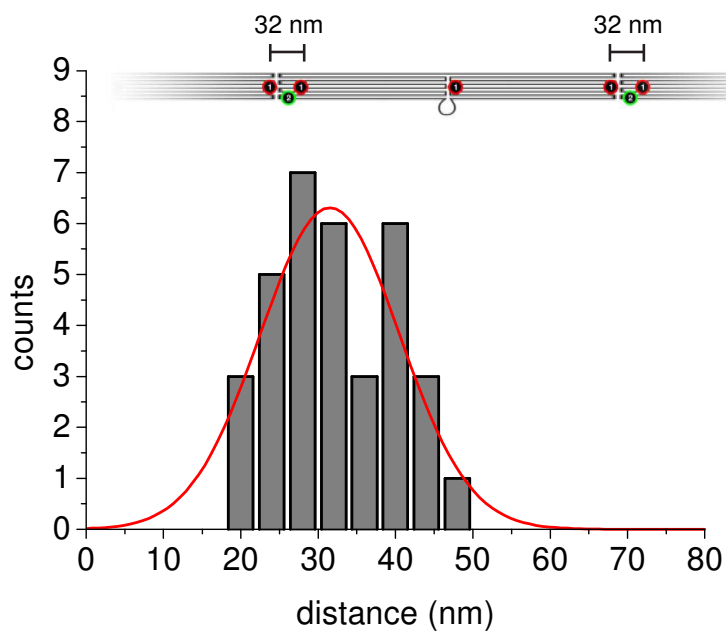


**Figure S6:** DNA-PAINT is able to resolve connection points on LR origami oligomers as close together as 32 nm. The distribution yields an experimentally determined distance of  $32.2 \pm 7.5$  nm ( $n = 34$ ).

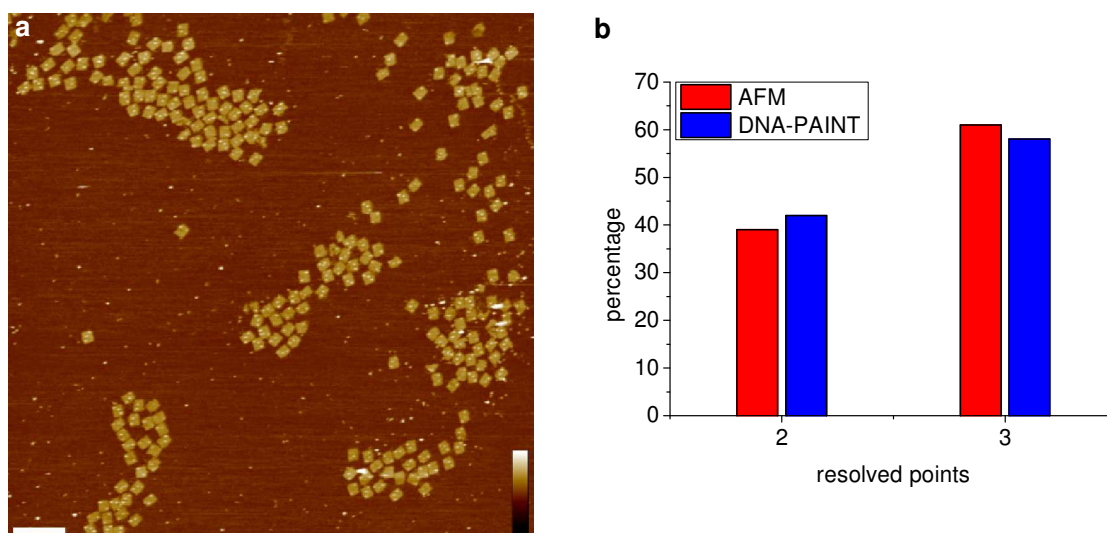


**Figure S7:** Efficiency of staple strand incorporation using 10x staple strand excess over the scaffold strand and imaging efficiency of DNA-PAINT. **a**, Typical AFM image of RROs carrying three biotinylated staple strands by design. Streptavidin was added in large excess (up to 200 ×) over the origami structures on the mica surface as well as in solution. Length scale: 400 nm, height scale: 10 nm. **b**, At a 10 x staple excess over the scaffold strand, the incorporation efficiency for three and two biotinylated staple strands was 61 % and 39 % respectively (n=392). DNA-PAINT was able to resolve three docking strand positions in 58 % and two in 42 % of the cases (n=73). This yields a high imaging efficiency of  $\approx 95$  %. Using a 100 × staple strand excess yielded an increase in incorporation efficiency to 83 % for three biotinylated determined by AFM imaging (data not shown).

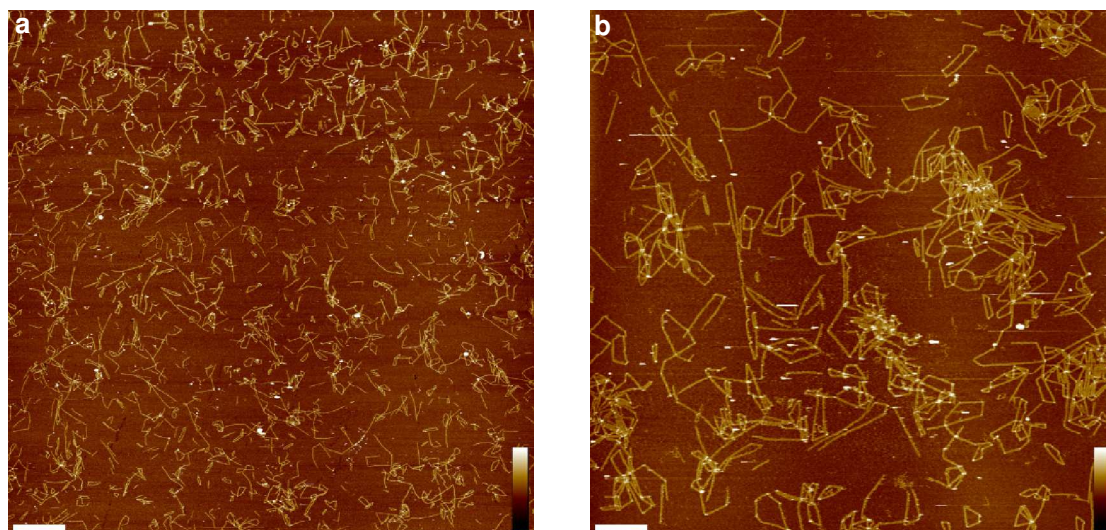


**Figure S8:** Additional liquid AFM images of LRO multimers. **a**, Length scale: 2  $\mu\text{m}$ , height scale: 6 nm. **b**, Length scale: 800 nm, height scale: 6 nm.





**Figure S9:** Detailed design schematics for the LR origami monomers and oligomers (for monomers, **multimerization strands** are omitted, discouraging unwanted, unspecific polymerization due to blunt-end stacking).

**Table S10:** DNA sequences for LR origami monomers, polymers, DNA-PAINT docking strands, biotin anchor strands, ATTO532 labeled strand, DNA-PAINT imager strand, DNA-PAINT surface immobilization strand.

Name	Sequence	Color	Comment
0 [15] 1 [863]	CAGCGAAAATAAATCCTCATTAATGATATTC		Multimerization
1 [864] 0 [16]	ACAAACAAGACAGCATCGGAACGAAACCTCAG		Multimerization
2 [15] 3 [863]	TAAATATTGACGGGAGAATTAACACAGGGAA		Multimerization
3 [864] 2 [16]	GCGCATTACATTGAATCCCCCTCAAATCGTCA		Multimerization
4 [15] 5 [863]	AGAGAATCCGCGAGAAAACCTTTTATCGCAAG		Multimerization
5 [864] 4 [16]	ACAAAGAAGATGAACGGTAATCGTAGCAACA		Multimerization
6 [15] 7 [863]	GGGAGAGGAATCAATATCTGGTCAAAAATATC		Multimerization
7 [864] 6 [16]	AAACCTCCGGTTTGCATATTGGGAACGCGCG		Multimerization
0 [47] 1 [31]	AAAGGCCGCTTTTGCGGGATCGTCGGGTAGCA		
0 [79] 1 [63]	ATATATTCGGTCGCTGAGGCTTGCAAAGACTT		
0 [111] 1 [95]	CAATGACAACAACCATCGCCACGCGGGTAAA		
0 [143] 1 [127]	CTTAAACAGCTTGATACCGATAGTCCAACCTA		
0 [175] 1 [159]	TCCGTTTATCAGCTTGCTTTCGAGCTAAAACA		
0 [207] 1 [191]	AAAAAAGGCTCCAAAAGGACCTTTACCAAGC		
0 [239] 1 [223]	AATAATAATTTTTTACAGTTGAAATGTATCAT		
0 [271] 1 [255]	GAGAATAGAAAGGAACAACCTAAAGCGCGACCT		
0 [303] 1 [287]	TGCTAAACAACCTTCAACAGTTTCAGGCGCAG		
0 [335] 1 [319]	ACGTTAGTAAATGAATTTTCTGTACTGACCAA		
0 [367] 1 [351]	CGTAACGATCTAAAGTTTGTGCTGTACAGA		
0 [399] 1 [383]	TGTAGCATTCCACAGACAGCCCTCTCATCAAG		
0 [431] 1 [415]	TGAGTTTCGTCACCACTACAACTTTCATTAC		
0 [463] 0 [432]	CAAGCCCAATAGGAACCCATGTACCGTAACAC		
0 [495] 1 [479]	CTCAGAGCCACCCTCATTTCCTCCGTCACC		
0 [527] 1 [511]	CCCTCAGAACCAGCCCTCAGAAAGCCAGCAA		
0 [559] 1 [543]	TATCACCGTACTCAGGAGTTTGTAGCAAGG		
0 [591] 1 [575]	AGGGTTGATATAAGTATAGCCCGTCGATAGC		
0 [623] 1 [607]	TGCTCAGTACCAGGCGGATAAGTGTCAAGTT		
0 [655] 1 [639]	CCTCAAGAGAAGGATTAGGATTAGCGTTTCA		
0 [687] 1 [671]	CTGAAACATGAAAGTATTAAGAGGTTATTAGC		
0 [719] 1 [703]	AATGCCCCCTGCCTATTTTCGAAACATCACCGG		
0 [751] 1 [735]	TGCCCTTGAGTAACAGTGCCCGTATCTCCCTCA		
0 [783] 1 [767]	AGTGTACTGGTAATAAGTTTAAACCCCTCAGA		
0 [815] 1 [799]	TAAGCGTCATACATGGCTTTGATAGAAACCAC		
0 [847] 1 [831]	GGAAAGCGCAGTCTCTGAATTTACCAGGAGGT		
1 [32] 3 [31]	ACGGCTACGCGTCCAATACTGCGGAATGCTTT		
1 [64] 3 [63]	TTTCATGAAGGGGTAATAGTAACCATATAAT		
1 [96] 3 [95]	ATACGTAAGCGAGAGGCTTTTGCATATTATAG		
1 [128] 3 [127]	AAACGAAATCGTTTACCAGACGACAAAAGATT		
1 [160] 3 [159]	CTCATCTTGAGGCATAGTAAGAGCATATCGCG		
1 [192] 3 [191]	GCGAAACATAATGCAGATACATAACAGACCG		
1 [224] 3 [223]	CGCCTGATATCAGTTGAGATTTAGTTAGAGAG		
1 [256] 3 [255]	GCTCCATGACGGAACAACATTATTAGAGGTCA		
1 [288] 3 [287]	ACGGTCAAGGAAGAAAATCTACGATTTGCTGA		
1 [320] 3 [319]	CTTTGAAAAGAAGTGGCTCATTATTTTAAATA		
1 [352] 3 [351]	CCAGGCGCTTAATCATTGTGAATTAGTTTCAT		
1 [384] 3 [383]	AGTAATCTTAAATTTGGGCTTGAGATCTGCGAA		
1 [416] 3 [415]	CCAAATCACTTGCCCTGACGAGAAGATACATT		
1 [448] 2 [432]	TTATTTCATAGGGAAGGTAATATTCATTCACT		
1 [480] 3 [479]	GACTTGAGAGACAAAAGGCGCACAAAGAAC		
1 [512] 3 [511]	AATCACCAAAATAGAAAATTCATATATCGAGAA		
1 [544] 3 [543]	CCGGAACACACCACGGAATAAGTCGTAGGAA		
1 [576] 3 [575]	AGCACCGTTAAAGGTGGCAACATAAAATCAGA		
1 [608] 3 [607]	TGCCTTTACAGTATGTTAGCAAACAAGAACC		
1 [640] 3 [639]	TCGGCATTAAGAACTGGCATGATTTTTCGCGG		
1 [672] 3 [671]	GTTTGCCACCGAGGAAACGCAATATTAGTTGC		
1 [704] 3 [703]	AACCAGAGGCAGATAGCCGAACAAATCCTGAA		
1 [736] 3 [735]	GAGCCGCTATCTTACCGAAGCCCTTCCAGAG		
1 [768] 3 [767]	GCCACCACATAAGAGCAAGAAACAACAGCCAT		
1 [800] 3 [799]	CACCAGAGGATAACCCACAAGAATAAACGATT		
1 [832] 3 [831]	TGAGGCAGGTGAGGGTAATTGAATAGCAGC		
2 [79] 0 [80]	TTTGCCAGGGAAGTTTCCATTAAACATAACCG		
2 [111] 0 [112]	CCAAAATATGCCACTACGAAGGCATGCGCCGA		
2 [143] 0 [144]	CATAACCCGAGGCAAAGAATACAGTGAATTT		
2 [175] 0 [176]	GGAATTACTGACCCCGAGGATTTATAATTTGTA		
2 [207] 0 [208]	CATTCAACAAGTACAACGGAGATTATCTCCAA		
2 [239] 0 [240]	AAAGATTCAAATTTGTGTCGAAATCGAATTCGG		
2 [271] 0 [272]	ACGAACTATTACTTAGCCGGAACGAGCGGAGT		
2 [303] 0 [304]	GGACGTTGTATAAGGGAACCGAATGGGATTT		
2 [335] 0 [336]	CGATTTTAGAGGACAGATGAACGGCTTTCCAG		
2 [367] 0 [368]	TTTCAACTATAGGCTGGCTGACCTATAGTTAG		
2 [399] 0 [400]	ACGAGTAGTGACAAGAACCAGGATAACAACGCC		
2 [431] 1 [447]	GAATAAGGACGTAACAAGCTGCTGACGGAAA		
2 [463] 0 [464]	ATTGAGGGTAAAGGTGAATATCAAGGGATAG		
2 [495] 0 [496]	AGCGCCAACCATTTGGGAATTAGACCGCCACC		

2 [527] 0 [528]	TCACAATCGTAGCACCATTACCATTACCGCCA
2 [559] 0 [560]	ACGCAAAGGTCACCAATGAAACCAATAGGTG
2 [591] 0 [592]	TACATACAAATCAGTAGCGACAGACCGTCGAG
2 [623] 0 [624]	TTATTACGGCGTCAGACTGTAGCGCGGGTTT
2 [655] 0 [656]	ATACCCAATTCGGTCATAGCCCCCTGAGACT
2 [687] 0 [688]	GAAGGAAATCTTTTCATAATCAAATATTATT
2 [719] 0 [720]	AAAAGTAACCACCACCGGAACCGCAAACAGTT
2 [751] 0 [752]	GCAATAGCACCCTCAGAACCGCCAGGGTCAG
2 [783] 0 [784]	GCCCAATACCTCAGAGCCGCCACCGATACAGG
2 [847] 0 [848]	TGAACAAAGTCAGACGATTGGCCTGCCAGAA
3 [32] 5 [31]	AAACAGTTTTGCGCTGAGAGTCTGAAAACTAG
3 [64] 5 [63]	CAAAAATCTTTTTGAGAGATCTACTGATAATC
3 [96] 5 [95]	TCAGAAGCAGCTGATAAATTAATGTTGTATAA
3 [128] 5 [127]	AAGAGGAAAAATCACCATCAATATAATATTTT
3 [160] 5 [159]	TTTTAATTATTCAAAGGGTGAGATTAATCA
3 [192] 5 [191]	GAAGCAAAAAATGCAATGCCTGAGGCCATCAA
3 [224] 5 [223]	TACCTTTAGGATAAAAAATTTTAGGTAGCCAG
3 [256] 5 [255]	TTTTTGCCTTTTTCGGGAGAAGCGAGTAACA
3 [288] 5 [287]	ATATAATGGGTTGTACCAAAAACAAACGGCG
3 [320] 5 [319]	TGCAACTAAGCAATAAAGCCTCAGCGTTGGTG
3 [352] 5 [351]	TCCAATACATACAGGCAAGGCAAAATCTGCCA
3 [384] 5 [383]	CGAGTAGAACTAATAGTAGTAGCAGGCCCTCAG
3 [448] 4 [432]	ATCGGCTGCGAGCATGTAGAAACCGACTATAT
3 [480] 5 [479]	GGTATTAAAGCAAGAAAAATAATCGGATTTCG
3 [512] 5 [511]	CAAGCAAGACGCGCCTGTTTATCAACAAAAATC
3 [544] 5 [543]	TCATTACCCGCAATAAACAACATAATTACCT
3 [576] 5 [575]	TATAGAAGCGCAAAAAGGTAAGTACATCAAG
3 [608] 5 [607]	GAGGCGTTTTTCGAGCCAGTAATAAATTTTCAT
3 [640] 5 [639]	AGGTTTTGACAACGCCCAACATGTACAGTACAT
3 [672] 5 [671]	TATTTTGCAGTAGGGCTTAATTTGCCTTGCTT
3 [704] 5 [703]	TCTTACCACAAATCTTACCAGTATTTTCCCT
3 [736] 5 [735]	CCTAATTTGAAAAAGCCTGTTTAGAGCTTAGA
3 [768] 5 [767]	ATTATTTAAATAAGAAATAAACCCGTGAATTT
3 [800] 5 [799]	TTTTGTTGAAATACCGACCGTGTACCTTTT
3 [832] 5 [831]	CTTTACAGAAATTCATCTTCTGACTATAACTA
4 [79] 2 [80]	GGTAGCTAAGGTCTTTACCCCTGACAAAGAA
4 [111] 2 [112]	ACCGTTCTAAAGCGGATTGCATCAGATAAAAA
4 [143] 2 [144]	AGACAGTCGCCGAAAGACTTCAAAACACTAT
4 [175] 2 [176]	AGGTAAGCGAGCTTCAAAGCGAACGCCAAAA
4 [207] 2 [208]	TATATTTTCTCCAACAGGTCAGGAGAATACCA
4 [271] 2 [272]	CTGTAATAGATGGCTTAGAGCTTATTAAATAA
4 [303] 2 [304]	GCTAAATCCTGTAGCTCAACATGTACCAGTCA
4 [335] 2 [336]	CAAAATTAAGTACGGTGTCTGGAACTTATG
4 [367] 2 [368]	CAATAAATACAGTTGATTCCCAATTTGGTTAA
4 [399] 2 [400]	TCAATTTCTTTTAGTTTGACCATTAACACCAGA
4 [431] 3 [447]	TTTCATTTGGTCAATAACCTGTTTAATCAATA
4 [463] 2 [464]	CTAATTTATCTTTCCCTTATCATTTCTTCAACCG
4 [495] 2 [496]	TAAGTCTTACCAAGTACCGCACTCGGTTTACC
4 [527] 2 [528]	AATGCAGACCGTTTTTATTTTCAATTTATTTTG
4 [559] 2 [560]	CCAGACGAGCGCCCAATAGCAAGCTAAAAGAA
4 [591] 2 [592]	TAAAATACGCTTATCCGGTATTCTGTAGAAAA
4 [655] 2 [656]	CATATTTAAAGCCTTAAATCAAGAAATAACGGA
4 [687] 2 [688]	ACGCTCAAACCCAGCTACAATTTTAGTTACCA
4 [719] 2 [720]	GCGTTATAACGCTAACGAGCGCTTTTTTAAG
4 [751] 2 [752]	AATTAAGTACGCTTACAAAAATAATGAAATA
4 [783] 2 [784]	AGGCGTTATCCCAATCCAAATAAGTGAGTTAA
4 [847] 2 [848]	TTTTAGTTAGAGAAATAACATAAAAAGAACCC
5 [64] 7 [63]	AGAAAAGCCTTTCCAGTCGGGAAACGGGCAAC
5 [96] 7 [95]	GCAAAATATACTCACATTAATTTGCGCCCTGAGA
5 [128] 7 [127]	GTTAAAATTTGTAAGCCTGGGGTGGGTTTGCC
5 [160] 7 [159]	GCTCATTTTTCCACACAACATACGTGGTGGTT
5 [192] 7 [191]	AAATAATTGTTTTCTGTGTGAAATAATCAAAA
5 [224] 7 [223]	CTTTCATCCCGAGCTCGAATTCGTGTTGTCC
5 [256] 7 [255]	ACCCGTGCGCTGCAGGTCGACTCTAAAGAAGC
5 [288] 7 [287]	GATTGACCTGTAAAACGACGGCCAAAACCGTC
5 [320] 7 [319]	TAGATGGGGGTAACGCCAGGGTTGAACCATC
5 [352] 7 [351]	GTTTGAGGGAAAGGGGATGTGCTGAGGTGCC
5 [384] 7 [383]	GAAGATCGGTGCGGGCCTCTTCGCAAGGGAGC
5 [448] 6 [432]	CTTTTACACAGATGAATATACAGTAAGCGCCA
5 [480] 7 [479]	CCTGATTGAAAGAAATTCGCTAGACAATATTA
5 [512] 7 [511]	GCGCAGAGATATCAAAATTTATTGACGCTCAT
5 [544] 7 [543]	GAGCAAAAATCTCTGAATAATGAAATCGTCT
5 [576] 7 [575]	AAAACAAATTCATCAATATAATCCATTCACCA
5 [608] 7 [607]	TTGAATTATCATCATATTTCTGATACATTTCTG
5 [640] 7 [639]	AAATCAATGAACAAAGAAACCCACCTGAAA
5 [672] 7 [671]	CTGTAATTTTTAAAAGTTTGTAGTAATTTTTT
5 [704] 7 [703]	TAGAATCCCGTATTAATCCTTTGCGAACTGA
5 [736] 7 [735]	TTAAGACGAAGTATTAGACTTTACAATACCGA
5 [768] 7 [767]	ATCAAAATGCCGTCAATAGATAATCAGAGGTG
5 [800] 7 [799]	TAACTCCTCTTTAGGAGCACTAAGCAACAGT
5 [832] 7 [831]	TATGTAAATTTGAAAGGAATTTGAGGTGAAAAAT
6 [47] 4 [48]	GCCAGCTGTCATATGTACCCCGTAAAGGCTA
6 [111] 4 [112]	GTGAGCTATTTAAATTTGTAACGTTGATATTCA
6 [175] 4 [176]	GCTCAAAATTTAACCAATAGGAACATAATGTGT
6 [303] 4 [304]	CACGACGTGTAATGGGATAGGTCAAGCATAAA
6 [367] 4 [368]	CAGCTGGCGGACGACGACGATCTTTAACATC
6 [431] 5 [447]	TTCCGCAATGCGGAAACAGGCAACAGTAC

SINGLE-MOLECULE KINETICS AND SUPER-RESOLUTION MICROSCOPY BY FLUORESCENCE IMAGING OF TRANSIENT BINDING ON DNA ORIGAMI - SUPPORTING INFORMATION

6 [495] 4 [496]	ACAGAAATCTTTGAATACCAAGTTACAATAGA		
6 [559] 4 [560]	TGGATTATGAAGATGATGAAACAAAATTCTGT		
6 [687] 4 [688]	TTATTAATCGTCGCTATTAATTAATAAGCCA		
6 [751] 4 [752]	GGATTAGCTGAGAAGAGTCAATAGGAATCAT		
6 [815] 4 [816]	CTAAAATAGGCTTAGGTTGGTTACTAAATTT		
7 [32] 6 [48]	TGGTTTTCTTTTCCACAGTGAGACCTGTCTGT		
7 [64] 6 [80]	AGCTGATTGCCCTTACCCTGGTTGCGCTC		
7 [96] 6 [112]	GAGTTGCAGCAAGCGTCCACGCTCCTAATGA		
7 [128] 6 [144]	CCAGCAGGCGAAAAATCCTGTTTGAAGCCGGAA		
7 [160] 6 [176]	CCGAAATCGGCAAAAATCCCTTATATGTTATCC		
7 [192] 6 [208]	GAATAGCCCGAGATAGGGTTGAGTAATCATGG		
7 [224] 6 [240]	AGTTTGGAAACAAGAGTCCACTATTAGAGGATC		
7 [256] 6 [272]	TGGACTCCAACGTCAAAGGGCGAAGTGCCAAG		
7 [288] 6 [304]	TATCAGGGCGATGGCCACTACGTTTCCCAAT		
7 [320] 6 [336]	ACCCAAATCAAGTTTTTGGGGTCGCAAGGCG		
7 [352] 6 [368]	GTAAGCACTAAATCGGAACCTATATTACGC		
7 [384] 6 [400]	CCCCGATTAGAGCTTGACGGGGATTGGGAAG		
7 [416] 7 [447]	GAACGTGGCGAGAAAGGAAGGAAACAACTAT		
7 [448] 6 [464]	CGCCTTGCTGGTAATATCCAGAATTTTCAGG		
7 [480] 6 [496]	CCGCCAGCCATTGCAACAGGAAAAACAGTAAA		
7 [512] 6 [528]	GGAAATACCTACATTTTGACGCTCAGGGTTAG		
7 [544] 6 [560]	GAAATGGATTATTACATTTGGCAGTGATTGTT		
7 [576] 6 [592]	GTCACACGACCAAGTAATAAAGGGTATCAGAT		
7 [608] 6 [624]	GCCAAACAGAGATAGAACCCTTCTGAGAAGGAG		
7 [640] 6 [656]	GCGTAAGAATACGTGGCACAGACAACATTATC		
7 [672] 6 [688]	GAATGGCTATTAGTCTTTAATGCGCCCGAAGC		
7 [704] 6 [720]	TAGCCCTAAAACATCGCCATTA AAAACAATT		
7 [736] 6 [752]	ACGAACCCAGCAGAAAGATAAAAAACATTTGA		
7 [768] 6 [784]	AGGGCGTCAAGTATTAAACCCGCTCAACTAAT		
7 [800] 6 [816]	GCCACGCTGAGAGCCAGCAGCAAAAAGTTAT		
7 [832] 6 [848]	CTAAAGCATCACCTTGCTGAACTGTTGGCAA		
3 [48] 1 [47]	TTTTGAGAATGAATGTTTAGACTGGATAAGAGGCTT		5'-Biotin
3 [816] 1 [815]	TTTTAAATGAAAAGCGCTAATATCAGAGACCGCCGCC		5'-Biotin
4 [415] 6 [416]	TTTTAGCTGAAACCGGCACCGCTTCTGGTCAGGCTG		5'-Biotin
5 [240] 3 [239]	TTTTATGTGAGCCTTATTTCAACGCAAATGTCTCC		5'-Biotin
5 [624] 3 [623]	TTTTAATGGAAAATTTAGGCAGAGGCATTTAGCGAA		5'-Biotin
5 [32] 7 [31]	TTTTCATGTCAACATTAATGAATCGGCCCGCCAGGG		5'-ATTO532
6 [79] 4 [80]	ACTGCCCGCCAAAAACAGGAAGACCGGAGAGTTATACATC		DNA-PAINT docking 7 bases
6 [143] 4 [144]	GCATAAAGTCGCATTAATTTTTGAAGCCGGTTATACATC		DNA-PAINT docking 7 bases
6 [207] 4 [208]	TCATAGCTCGCGTCTGGCCTTCTAACCCCTCATATACATC		DNA-PAINT docking 7 bases
6 [271] 4 [272]	CTTGCAATGGATTCTCCGTGGGAACTTATGACCTTATACATC		DNA-PAINT docking 7 bases
6 [335] 4 [336]	ATTAAGTTCGCATCGTAACCGTGCAGAAATAGTTATACATC		DNA-PAINT docking 7 bases
6 [399] 4 [400]	GGCGATCGCACTCCAGCCAGCTTTAGTTGGCATTATACATC		DNA-PAINT docking 7 bases
6 [463] 4 [464]	TTTAACGTTCCGGGAGAAAACAATAAATCCCATCTTATACATC		DNA-PAINT docking 7 bases
6 [527] 4 [528]	AACCTACCGCAATTATTCATTTTCGTTTCAGCTTATACATC		DNA-PAINT docking 7 bases
6 [591] 4 [592]	GATGGCAAATTAATTACATTTAACAGAGAATATATATACATC		DNA-PAINT docking 7 bases
6 [655] 4 [656]	ATTTTGGGATATGTGAGTGAATAAAGAATCGCTTATACATC		DNA-PAINT docking 7 bases
6 [719] 4 [720]	CGACAACCTTGA AAAACATAGCGATTATCATATTTATACATC		DNA-PAINT docking 7 bases
6 [783] 4 [784]	AGATTAGACATAGGTCTGAGAGACGATAAATATATATACATC		DNA-PAINT docking 7 bases
6 [847] 4 [848]	ATCAACAGTGCTGATGCAAATCCACAAATATATATACATC		DNA-PAINT docking 7 bases
6 [79] 4 [80]	ACTGCCCGCCAAAAACAGGAAGACCGGAGAGTTATACATCTA		DNA-PAINT docking 9 bases
6 [463] 4 [464]	TTTAACGTTCCGGGAGAAAACAATAAATCCCATCTTATACATCTA		DNA-PAINT docking 9 bases
6 [847] 4 [848]	ATCAACAGTGCTGATGCAAATCCACAAATATATATACATCTA		DNA-PAINT docking 9 bases
6 [463] 4 [464]	TTTAACGTTCCGGGAGAAAACAATAAATCCCATCTTATACATCTAG		DNA-PAINT docking 10 bases
DNA-PAINT-imager	CTAGATGTAT	n/a	3'-A655 or 3'-Cy3B
DNA-PAINT-immo	TTATACATCTAG	n/a	5'-Biotin

**Table S11:** Modified DNA sequences for RR origami: DNA-PAINT docking strands, biotin anchor strands, Cy3b labeled strand. Nomenclature according to Rothemund's original design<sup>1</sup>.

Name	Sequence	Comment
r-5t4f_6f	TTTTTCGAAATCTGTACAGACCAGGCGCTTAATCAT	5'-Biotin
r5t18f_20f	TTTTATTATTTGACATTATCATTTCGCGCTTTAGG	5'-Biotin
r-1t14f_16f	TTTTCATCAATATAATATTTGTAAAAATTTAACC	5'-Biotin
r-5t20f_22f	TTTTTCGGGAAACGGGCAACAGCTGATTACAAGAGT	5'-Biotin
r5t4e_6e	TTTTCAGCATTGACGTTCCAGTCACAATCGTAGCACC	5'-Biotin
r1t12f	ATCGGCTGCGAGCATGTAGAAACCAGCTATATTTATACATCTA	DNA-PAINT docking 9 bases
r7t4e	TGCCTTTAGTCAGACGATTGGCCTGCCAGAATTTATACATCTA	DNA-PAINT docking 9 bases
r-7t2e	TTTTAAAGGCCGAAAGGAACAACAACTAAAGCTTCCAG	5'-Cy3b

## References

1. Douglas, S. M.; Dietz, H.; Liedl, T.; Högberg, B.; Graf, F.; Shih, W. M. *Nature* **2009**, 459, (7245), 414-418.
2. Steinhauer, C.; Jungmann, R.; Sobey, T.; Simmel, F.; Tinnefeld, P. *Angewandte Chemie-International Edition* **2009**, 48, 8870-8873.
3. Steinhauer, C.; Forthmann, C.; Vogelsang, J.; Tinnefeld, P. *Journal of the American Chemical Society* **2008**, 130, (50), 16840-16841.
4. Mathe, J.; Visram, H.; Viasnoff, V.; Rabin, Y.; Meller, A. *Biophysical Journal* **2004**, 87, (5), 3205-3212.
5. Anshelevich, V. V.; Vologodskii, A. V.; Lukashin, A. V.; Frankkamenetskii, M. D. *Biopolymers* **1984**, 23, (1), 39-58.
6. Vogelsang, J.; Kasper, R.; Steinhauer, C.; Person, B.; Heilemann, M.; Sauer, M.; Tinnefeld, P. *Angew Chem Int Ed* **2008**, 47, 5465-5469.
7. Rothemund, P. W. K. Folding DNA to create nanoscale shapes and patterns. *Nature* **440**, 297-302.



# Curriculum Vitae

## Christian Steinhauer

Date of birth 31.03.1982  
Place of birth Heidenheim a. d. Brenz, Germany  
Nationality German  
Marital status married

## Education

2007–today **Doctoral program**, *Ludwig-Maximilians-Universität, Munich*.  
Faculty of Physics  
2005–2006 **Study abroad**, *University of Adelaide, Adelaide*.  
2002–2007 **Diploma in Molecular Biotechnology**, *Universität Bielefeld*.  
Technical Faculty  
2001–2002 **Civil Service**, *Ev. Jugendwerk, Heidenheim*.  
2001 **Abitur**, *Hellenstein Gymnasium, Heidenheim*.

## Work experience

2007–today **Doctoral program**, *Ludwig-Maximilians-Universität, Munich*.  
Faculty of Physics, Chair of Applied Physics – Biophysics, AG Prof. Tinnefeld  
2006–2007 **Student research assistant**, *Universität Bielefeld, Faculty of Physics*.  
Setting up a biological laboratory for the expression of recombinant proteins.  
2005–2006 **Research technical officer**, *CYWHS, Matrix Biology Lab, Adelaide*.

## Fellowships and awards

Presentation award Student presentation award at the Australian Institute of Physics congress in 2010.  
Doctoral fellowship Doctoral fellowship by the International Doctorate Program Nano-Biotechnology financed by the Elite Network of Bavaria.  
Publication award Three awards in 2009 and 2010 for collaborative and high-impact publications by the Center for NanoScience at the LMU.  
Seed funding Seed funding for US collaboration and the DNA origami project from the Nanosystems Initiative Munich.

Moosfeldstr.2 – 85238 Petershausen

☎ +49176 20 700 478 • ☎ +498137 62 90 79 • 📠 +498137 53 85 82  
• ✉ christian.steinhauer@gmail.com

## Soft skills

- Conflict management Four day seminar on conflict management and mediation by the Elite Network of Bavaria
- Entrepreneurship Three day seminar on patents and how to start a business by the Entrepreneurship Center of the LMU

## Conferences and workshops

- 2010 Australian Institute of Physics Congress, Australia (Contributed Talk)  
Gordon Research Conference: Single Molecule Approaches To Biology, Italy (Poster)  
4th Annual Symposium on Nanobiotechnology, Germany (Poster)  
Picoquant Workshop: Single Molecule Spectroscopy and Ultrasensitive Analysis in life sciences, Germany (Contributed Talk)
- 2009 Vielberth-Symposium on Functional Nucleic Acids, Germany (Poster)  
Foundations of Nanoscience, USA (Poster)  
Nano-Biotechnology and Complex Interfaces winter school, Italy (Talk)
- 2008 European Workshop on Advanced Fluorescence Imaging and Dynamics, Germany  
Center for Nanoscience workshop: Complex nanosystems: assembly, control and functionality, Italy (Poster)
- 2007 Picoquant Workshop: Single Molecule Spectroscopy and Ultrasensitive Analysis in life sciences, Germany
- 2006 Annual Meeting of the Matrix Biology Society of Australia and New Zealand, Australia (Poster)

Moosfeldstr.2 – 85238 Petershausen

☎ +49176 20 700 478 • ☎ +498137 62 90 79 • ☎ +498137 53 85 82  
• ✉ christian.steinbauer@gmail.com

**Full list of Publications**

I.H. Stein, **C. Steinhauer** and P. Tinnefeld. Four-color Single-Molecule FRET visualizes Energy Transfer Paths on DNA Origami. Submitted to *J Am Chem Soc*.

**C. Steinhauer**, C. Forthmann, R. Jungmann, J. Vogelsang, F.C. Simmel and P. Tinnefeld. Nanoscopy Using Localization and Temporal Separation of Fluorescence from Single Molecules; in *Biophotonics: Spectroscopy, Imaging, Sensing, and Manipulation*, NATO Science for Peace and Security Series B: Physics and Biophysics, B. D. Bartolo, J. Collins (Eds.), Springer, 87-106, 2011.

R. Jungmann\*, **C. Steinhauer\***, M. Scheible, A. Kuzyk, P. Tinnefeld, and F. C. Simmel. Single-molecule kinetics and super-resolution microscopy by fluorescence imaging of transient binding on DNA origami. *Nano Lett* 10(11):4756-4759, Oct 2010. \*equal contribution

J. Vogelsang, **C. Steinhauer**, C. Forthmann, I. H. Stein, B. Person-Skegro, T. Cordes, and P. Tinnefeld. Make them blink: probes for super-resolution microscopy. *ChemPhysChem*, 11(12):2475-2490, Aug 2010.

J. Vogelsang, T. Cordes, C. Forthmann, **C. Steinhauer**, and P. Tinnefeld. Intrinsically resolution enhancing probes for confocal microscopy. *Nano Lett*, 10(2):672-679, Feb 2010.

T. Cordes, M. Strackharn, S. W. Stahl, W. Summerer, **C. Steinhauer**, C. Forthmann, E. M. Puchner, J. Vogelsang, H. E. Gaub, and P. Tinnefeld. Resolving single-molecule assembled patterns with superresolution blink-microscopy. *Nano Lett*, 10(2):645-651, Feb 2010.

**C. Steinhauer\***, R. Jungmann\*, T. L. Sobey, F. C. Simmel, and P. Tinnefeld. DNA origami as a nanoscopic ruler for super-resolution microscopy. *Angew Chem Int Ed Engl*, 48(47):8870-8873, Oct 2009. \*equal contribution

B. Person, I. H. Stein, **C. Steinhauer**, J. Vogelsang, and P. Tinnefeld. Correlated movement and bending of nucleic acid structures visualized by multicolor single-molecule spectroscopy. *ChemPhysChem*, 10(9-10):1455-1460, Jul 2009.

J. Vogelsang, T. Cordes, C. Forthmann, **C. Steinhauer**, and P. Tinnefeld. Controlling the fluorescence of ordinary oxazine dyes for single-molecule switching and superresolution microscopy. *Proc Natl Acad Sci U S A*, 106(20):8107-8112, May 2009.

**C. Steinhauer**, C. Forthmann, J. Vogelsang, and P. Tinnefeld. Superresolution microscopy on the basis of engineered dark states. *J Am Chem Soc*, 130(50):16840-16841, Dec 2008.

J. Vogelsang, R. Kasper, **C. Steinhauer**, B. Person, M. Heilemann, M. Sauer, and P. Tinnefeld. A reducing and oxidizing system minimizes photobleaching and blinking of fluorescent dyes. *Angew Chem Int Ed Engl*, 47(29):5465-5469, 2008.